Theoretical study on a plastic phase of ice

Kazuhiro Himoto

Graduate School of Natural Science and Technology
Okayama University
March 2014

INDEX

ACKNOWLEDGMENTS

Thanks to the support of many people, I was able to finish writing this dissertation and spent a productive academic life. I genuinely express my gratitude to them.

Hideki Tanaka.

As my primary mentor and also supervisor, Professor Hideki Tanaka has supported me in both my academic life and research since I was an undergraduate student. I cannot thank him enough.

Masakazu Matsumoto.

Professor Masakazu Matsumoto, my supervisor and also mentor, is the one who has affected me the most in my academic life. He has guided and helped me with my works. He has taught me many development techniques, such as programming, paper writing, graphic design etc.

Kenichiro Koga.

Professor Kenichiro Koga, my mentor, taught me statistical mechanics. He has given me many helpful comments regarding my study.

Wakako Tsukiashi.

I acknowledge the office administrator, Ms. Wakako Tsukiashi, for her great support throughout my entire graduate student life.

Members of Laboratory of Theoretical Chemistry; My Colleagues; My Friends.

I wish to express my gratitude to Professor Lukman Hakim, Mr. Takato Nakayama, Mr. Kiharu Abe, Dr. Noriko Yamamoto, Dr. Kenji Mochizuki, Dr. Ryoji Mitsuhashi, and Ms. Nozomi Adachi. Thanks to them, I have been able to spend enjoyable, enthusiastic, and happy academic life as a graduate student.

Japan Society for the Promotion of Science (JSPS).

I thank Japan Society for the Promotion of Science (JSPS) for its support by *Research Fellowship for Young Scientist*.

My Family.

I would like to express my deepest gratitude to my mother, Takako. Her support and love have been strongly encouraged me as I have struggled to get a Ph.D. and to go beyond it. I thank my grandmothers, Kieko Mori and Akiko Himoto; my brother, Kohei; my father, Eisuke; and all my family, who have watched over me.

This dissertation is dedicated to my late grandfathers Sugio Mori and Yasuo Himoto, and to all my family.

Chapter 1

General introduction

1.1 Ice VII: a polymorph of ice

There is no material that has the greater number of structural forms than that of water. Experimentally, so far, 16 different crystalline ice phases ("the polymorphism of ice") have been confirmed to exist [1]. The crystalline ices identified by experiments have been assigned numbers, such as ice I*h*, I*c*, II, and the latest XV. The ice polymorph comprises metastable ices and non-molecular ones as well as stable molecular crystals: ices I*c,* IV, IX, XII, and XIV are molecular metastable phases; ices X and XI[1] are non-molecular stable phases. It was very recent that the latest-found ice, ice XV, was identified by Saltzmann et al. [2]. Therefore, there is a strong likelihood that yet another ice phases are latent in phase diagram. Updating water's phase diagram (Fig. 1.1(a)) is still one of the most challenging and significant scientific themes.

---

[1] There is confusion in allocating the number XI; one for proton-ordered form of ice Ih and another for hexagonal ice of symmetrized proton.

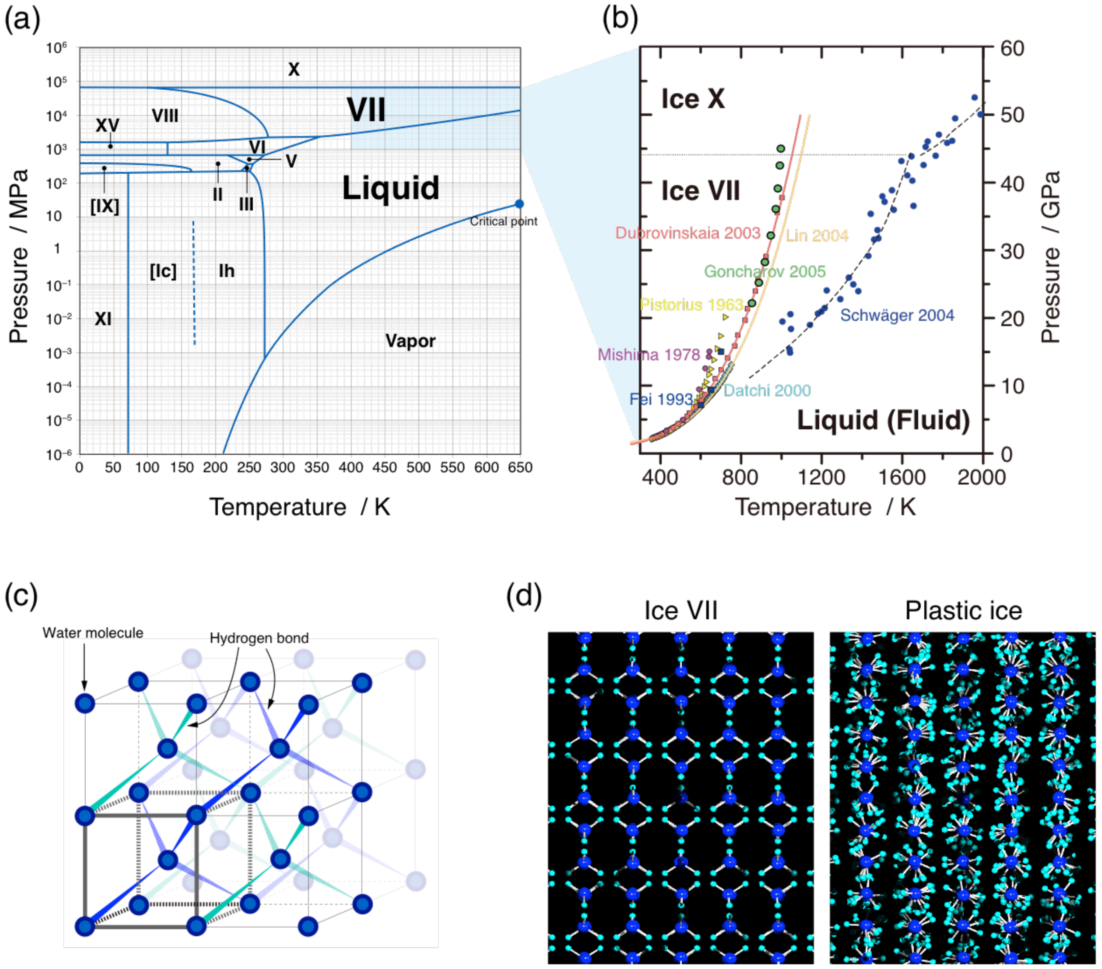

Figure 1.1

(a) The phase diagram of water. Some ice phases are not shown. With bracket corresponds to metastable phase.

(b) The prior experimental melting curves of ice VII [3–10]. Each label for plot indicates the first author and the publication year of the paper.

(c) The unit-cell structure of ice VII. Sphere is the position of a water molecule. The two hydrogen-bond networks are depicted by blue and cyan lines.

(d) Orthographic snapshots of ice VII (left) and plastic ice (right). Blue spheres are oxygen atoms and cyan ones are hydrogen atoms. No hydrogen bond is drawn. The lattice structure in plastic ice is the same as that in ice VII, but plastic ice does not have hydrogen-bond network due to its almost-free molecular rotation.

Water preserves its molecular framework up to about 20 GPa. The most dense ices in molecular crystalline phases are ice VII and ice VIII, which coexist at a pressure higher than ~2 GPa in the phase diagram, as shown in Fig. 1.1. Ice VII is a self-clathrate, where proton-disordered two diamond-type hydrogen-bond networks interpenetrate each other (Fig.1.1(c)). On the other hand, in terms of molecular configuration, the unit cell of its lattice structure is body-centered cubic (BCC) lattice. Ice VIII is the proton-ordered counterpart of ice VII, whose lattice has a lower symmetry and is tetragonal.

The first report of the existence of ice VII dated back to 1937, by Bridgman [11]. Since then, however, the melting curve of ice VII has yet to be settled by experimental works [3–10,12]. The different experimental methods have resulted in the different melting curves and the discrepancy spreads wider as pressure increases. Several prior experimental melting curves of ice VII are collected in Fig. 1.1(b). Most of the earlier experimental works evaluated the melting points by the change in the volume of system, while most of the late experimental surveys on the melting of ice VII were made by direct (visual) observation. Differences among methods make it difficult to identify the correct melting curve.

1.2 The appearance of plastic ices in computer simulation

In 2008, Takii, Koga, and Tanaka suggested a distinct interpretation as to the problem that the melting curve of ice VII had not been identified [13]. Their report stated that when ice VII is heated in molecular dynamics (MD) simulation, it melts not to liquid but to plastic phase, in which each molecule can rotate freely but cannot move away from certain lattice point (Fig.1.1(d)). Although there are many kinds of materials that possess plastic phase [14], the report by Takii et al. (Ref. [13]) is the first one regarding the plastic phase of water. The tentative name for the plastic phase of water is “plastic ice,” which has no official name because of the lack of experimental identification.

Computational results and various analyses in the paper of Takii et al. strongly encourage the possibility for the existence of plastic ice [13]. Moreover, in 2009, Aragones et al. conducted the further computer simulations so as to confirm the plastic ice; and they also found, in higher-pressure region, another plastic ice whose structure differs from what Takii et al. had reported [15,16]. That the experiments have not taken the plastic phase of ice into account may be a reason for the discrepancy of the experimental melting curves of ice VII. Therefore, it is anticipated that this research field will become more active increasingly.

1.3 Overview of the dissertation

The keywords in this dissertation are plastic ice and ice VII. The main topics are structural differences, energetic differences, dynamic differences, and the phase transition behavior between those two ice phases. This dissertation consists of this chapter and our research outcomes (Chapters 2 through 4).

In Chapter 2, I report energetic and microscopic structural differences between plastic ice and ice VII, and the feature in terms of hydrogen bond in plastic ice. At non-zero temperature, the system continually moves on complicated potential energy landscape. At a basin on the potential energy landscape at which the structure is called "inherent structure [17]" or "Q-structure[2]," the thermal noise is eliminated and accordingly the HB network becomes clear [17–19]. We compare the inherent structures of plastic ice and ice VII, whose densities are the same as one another. We show that the isotropic short-range repulsive interaction term's contribution is greater than the Coulombic interaction term, in the total potential energy which is the sum of those terms. (Concerning the water's intermolecular potential function model is described in Appendix for Chapter 1.) Our survey also reveals that the BCC configurations of plastic ice and ice VII are quite different at microscopic level, according to the average deviation from the perfect BCC lattice point whose density is the same as those phases. Moreover, it is found that even though the lattice structure of plastic ice is BCC, as with ice VII, the total number of HBs in the plastic ice system is much smaller than that in ice VII and there are various hydrogen-bonding patterns per molecule not restricted to four tetrahedral directions in plastic ice.

In Chapter 3, we investigate the reorientational autocorrelations and the hydrogen-bond autocorrelations of plastic ice, ice VII, and liquid water to evaluate the

---

[2] Potential energy minimization so as to find a structure at a basin on the potential energy landscape (i.e., an inherent structure) is also often called "*quenching*." The name "Q-structure" originates in the "*q*"uenching and is used in Chapter 2.

association between molecular rotation and energetic relaxation. We check that the hydrogen-bond autocorrelation of plastic ice decays like liquid and then settle into the non-zero value like crystalline phase, reflecting the free rotation and impermissible diffusion of water molecule in plastic ice. Also checked is that the lifetime of HB depends only on the molecular rotational motion, according to the similarity between the reorientaional and the HB correlations.

Finally, in Chapter 4, I show that, in computer simulation, the phase boundary between ice VII and plastic ice switches itself from first-order transition line (*coexistence* line) to second-order phase transition line (*critical* line) and these boundaries are joined by a tricritical point. So far, researchers have concluded that the phase transition between ice VII and plastic ice is entirely first-order transition due to the observation of hysteresis in thermodynamic quantity profile and the intersection of chemical potential profile. We perform the vast number of MD simulations in very wide range of pressure, then observing the critical phenomena such as the divergent behavior of the heat capacity at constant pressure as a function of temperature in higher-pressure region. We obtain the typical critical exponents and those exponents satisfy a “scaling law” which should holds at a critical point. Furthermore, the scaling raw here is confirmed to hold regardless of pressure, from 10 to 26 GPa. In addition to those results, analyzing a Landau’s phenomenological free energy enables us to find that a tricritical point joins the coexistence and critical lines and to estimate the location of the tricritical point in the phase diagram at (temperature, pressure) = (665 K, 13.3 GPa). The critical behavior on the VII-plastic phase boundary is the third one following the trivial liquid-vapor critical phenomena and the hypothetical liquid-liquid critical phenomena in the supercooled region.

Appendix for Chapter 1

The classical intermolecular potential models of water.

Here I describe about the water models to simulate water's properties computationally. Molecular dynamics simulation is a technique to reproduce the time development of the system, where the molecules are moved with obeying the Newton's equations of motion,

$$m_i \frac{\mathrm{d}^2 \mathbf{r}_i}{\mathrm{d}t^2} = -\sum_j \frac{\partial \phi_{ij}}{\partial (\mathbf{r}_j - \mathbf{r}_i)}, \tag{A1.1}$$

where $\mathbf{r}_i$ is the position vector of *i*-th molecule, m_i the mass of *i*-th molecule, and ϕ_{ij} the pair potential energy between *i*- and *j*-th molecules. Numerical integration of the Eq. A1.1 gives the $\mathbf{r}_i$ in the future. So as to do the numerical integration, one needs to give ϕ_{ij} as an analytical form in advance. For water, ϕ_{ij} is often given by

$$\phi_{ij} = \sum_{ab} \frac{q_a q_b}{r_{ab}} + 4\epsilon \left[\left(\frac{\sigma}{r_{\mathrm{OO}}} \right)^{12} - \left(\frac{\sigma}{r_{\mathrm{OO}}} \right)^{6} \right]. \tag{A1.2}$$

The first term in the right side is the Coulombic potential term and the second term is ("12-6 type") Lennard-Jones potential term. The parameters q_a and q_b, are the charges on the sites *a* and *b*, respectively; the notation of summation means the sum for all possible $\{a, b\}$ pairs. ϵ and σ in the second term are also parameters. r_{OO} is the distance between oxygen atoms in *i*- and *j*-th water molecules.

No model can reproduce the whole water's properties or phase diagram precisely. In Eq. A1.2 for the water models such as TIP4P, TIP5P, and so on, the parameters q_a (q_b), ϵ and σ are optimized so as to reproduce particular properties —– for example, the maximum density of liquid water at 4°C —– as well as possible. The parameters for the rigid (i.e., the molecular framework is completely fixed) models[3], TIP3P[4] [20],

---

[3] There are the models whose OH bond's stretching and HOH angle's bending are permitted (so-called the flexible models).

[4] "TIP" is abbreviated from "Transferable Intermolecular Potential" and "3P" is from "3-Point" sites.

TIP4P [20], TIP4P/2005 [21], TIP5P [22], and TIP5P-E [23] are tabulated in Table A1.1. Also, the molecular geometries including negative charge sites for 3-site (TIP3P), 4-site (TIP4P and TIP4P/2005) and 5-site (TIP5P and TIP5P-E) models are illustrated in Fig. A1.1.

Table A1.1

Parameters and molecular geometry for the potential functions of 3-site (TIP3P), 4-site (TIP4P and TIP4P/2005), and 5-site (TIP5P and TIP5P-E) rigid water models. q_{H} is the proton charge, r_{OH} is the length of the OH bond, θ_{HOH} is the HOH angle, r_{OL} is the distance from O to a negative charge site (denoted by "L" here), θ_{LOL} is the LOL angle. The illustrations for these models are given in Fig. A1.1.

	3-site model	4-site		5-site	
	TIP3P	TIP4P	TIP4P/2005	TIP5P	TIP5P-E
q_{H} / e	0.417	0.520	0.5564	0.241	0.241
σ / Å	3.15061	3.15365	3.1589	3.12	3.097
ϵ / kcal mol^{-1}	0.1521	0.1550	0.18520	0.16	0.178
r_{OH} / Å	0.9572	0.9572	0.9572	0.9572	0.9572
θ_{HOH} / deg	104.52	104.52	104.52	104.52	104.52
r_{OL} / Å		0.15	0.1546	0.70	0.70
θ_{LOL} / deg				109.47	109.47

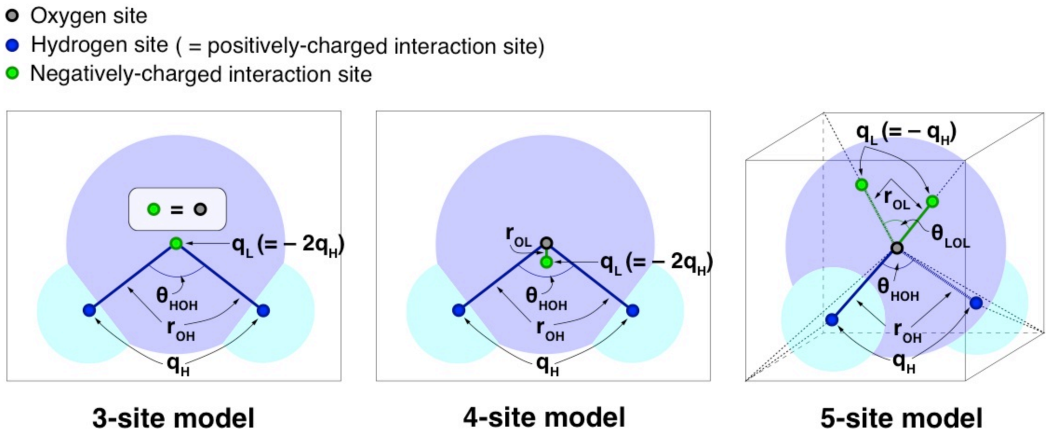

Figure A1.1

Illustrations for geometries of the 3-site (TIP3P), 4-site (TIP4P and TIP4P/2005), and 5-site (TIP5P and TIP5P-E) rigid models. In all of these models, positive charges (q_{H}) are placed on the two hydrogen atoms. TIP3P model has a negatively-charged (q_{L}) interaction site on oxygen atom. TIP4P and TIP4P/2005 have a negatively-charged (q_{L}) interaction site on dipole vector. TIP5P and TIP5P-E have two negatively-charged (q_{L}) sites on tetrahedral directions. All these models do not have polarization, that is, $q_{\mathrm{L}} = -2q_{\mathrm{H}}$ for TIP3P, TIP4P and TIP4P/2005; $q_{\mathrm{L}} = -q_{\mathrm{H}}$ for TIP5P and TIP5P-E. The values for the bond lengths, the angles, and so on in this picture are tabulated in Table A1.1.

Chapter 2

Lattice- and network-structure in plastic ice

We have investigated structural and energetic characteristics of plastic ice, which was found in a high-pressure region such as 10 GPa by molecular dynamics simulation and free energy calculation. It was predicted that plastic ice intervenes between ice VII and liquid water, in which diffusion is suppressed but rotation is allowed. In the present work, the structure in plastic ice is explored from both local and global view points and focus is placed on the local arrangement, the extent of deviation from the ideal lattice position, and the hydrogen-bonded patterns. The roles of the attractive interaction and the repulsive part of Lennard-Jones potential are also examined. It is found that the higher interaction energy in plastic ice induces a large dislocation of water molecules, which eventually conducts a facile rotation. There are a large amount of hydrogen-bonds which do not orient to the tetrahedral directions. These orientational defects give rise to fusion of the two interpenetrating sublattices of ice VII leading to a plastic phase rather than defect-containing ice VII, which results in a unique network structure of the plastic ice.

2.1 Introduction

Water exhibits a rich variety of phase behavior in a wide range of temperature and pressure, having more than 16 morphologies [2,24–26]. It freezes to a high density ice form, called ice VII at a pressure above 2 GPa [27–31]. Ice VII has the highest density made of intact water molecules. Its structure is identified with a body-centered cubic (BCC) lattice, in which each water molecule is hydrogen-bonded with half of the nearest neighbors. Thus, it can be viewed as a kind of self-clathrate composed of two interpenetrating cubic ice (ice I*c*) lattices [32]. For pressures lower than 20 GPa, the molecular framework of water is well preserved so that its local structure is dominated by hydrogen bonds (HBs) with four neighbors as well as the packing efficiency [27,28].

A plastic phase is an unusual solid state found for some substances in which molecules rotate nearly freely at lattice sites [33]. Takii et al. found a plastic phase of water by molecular dynamics simulations and free energy calculations with various intermolecular potential functions [13], TIP4P [20], TIP5P [22], SPC/E [34], and a polarizable model [35] in the framework of rigid molecules under several system sizes from N (number of water molecules) = 432 to 3456. A plastic phase emerges irrelevant to the boundary conditions, upon application of either short-range truncation [36] or the Ewald sum method [37]. This phase appears at a fairly high density that suppresses diffusional motions unlike the case of low pressure ices including ice I*c*. A nearly spherical shape of water molecules seems to facilitate rotational motions by breaking some of HBs but avoids a melting transition to liquid. Also found was a plastic phase of face-centered cubic (FCC) lattice for a water-like model with sluggish HBs.

Similar studies were made in order to include the plastic phase in the phase diagram of water using a variant of the TIP4P water called TIP4P/2005 [21] by a different method to calculate the phase boundary [15,16]. They also found an FCC plastic phase at a much higher pressure. The FCC phase seems to be associated with what was found for a water-like model with sluggish HBs.

Although it is of great importance to elucidate the difference between crystalline and plastic ice from a view point of the local and global network structures, no such microscopic picture has been established. In the present work, we investigate structural and energetic characteristics of the plastic ice by exploring the local arrangement, the extent of deviation from the ideal lattice position, and the hydrogen-bonded patterns in the plastic ice.

2.2 Methods

Isothermal-isobaric molecular dynamics simulations are performed to compare the structures and thermodynamic properties of liquid, plastic, and crystalline phases under 12 GPa. The TIP5P water model is employed and the long-range interaction is truncated smoothly at 0.8655 nm [36]. As the initial structure, 432 water molecules are placed on BCC lattice sites in the cubic simulation cell with periodic boundary conditions. Long-time simulations are performed at three different temperatures, 500, 640 and 960 K. After 8 ns run for equilibration, ice VII, plastic, and liquid phases are obtained, respectively. 100 independent instantaneous structures, say I-structures, are extracted at each temperature. The mean densities of ice VII, plastic phase, and liquid phase are 1.8703 g cm^{-3}, 1.7699 g cm^{-3}, and 1.6393 g cm^{-3}, respectively. All the structures are then scaled in size so that the density becomes the mean value at the plastic phase, 1.7699 g cm^{-3}, in order to remove the effect by volume difference in potential energy analysis discussed in the next section. Finally, 100 inherent structures, say Q-structures, are obtained for each temperature by the steepest descent method.

2.3 Results and Discussion

2.3.1 Identification of plastic phase and thermodynamic properties

Identification of water as a plastic phase is made by two time correlation functions namely the mean square displacement and the reorientational correlation function according to the definition of a plastic phase. These are defined by

$$Z_{\mathrm{t}}(t) \equiv \left\langle \frac{1}{N} \sum_{i=1}^{N} |\mathbf{r}_i(t) - \mathbf{r}_i(0)|^2 \right\rangle \tag{2.1}$$

for the mean square displacement, where $\mathbf{r}_i(t)$ stands for a center of mass coordinate of molecule i at time t, and

$$Z_{\mathrm{r}}(t) \equiv \left\langle \frac{1}{N} \sum_{i=1}^{N} |\mathbf{u}_i(t) \cdot \mathbf{u}_i(0)|^2 \right\rangle \tag{2.2}$$

for the reorientational correlation function, where $\mathbf{u}_i(t)$ stands for a unit vector parallel to a dipole of water molecule i at time t. Those time correlation functions are depicted in Fig. 2.1. We recover the same temperature dependence of these time correlation functions as that initiated with different coordinates reported previously [13]. The plastic phase emerges in the tem- perature range between 590 and 890 K for heating while its range is a little narrower in cooling at 10 GPa. That is caused by the hysteresis in transition between plastic and liquid. Here, we set the pressure to 12 GPa so as to observe a facile transition in heating and cooling processes.

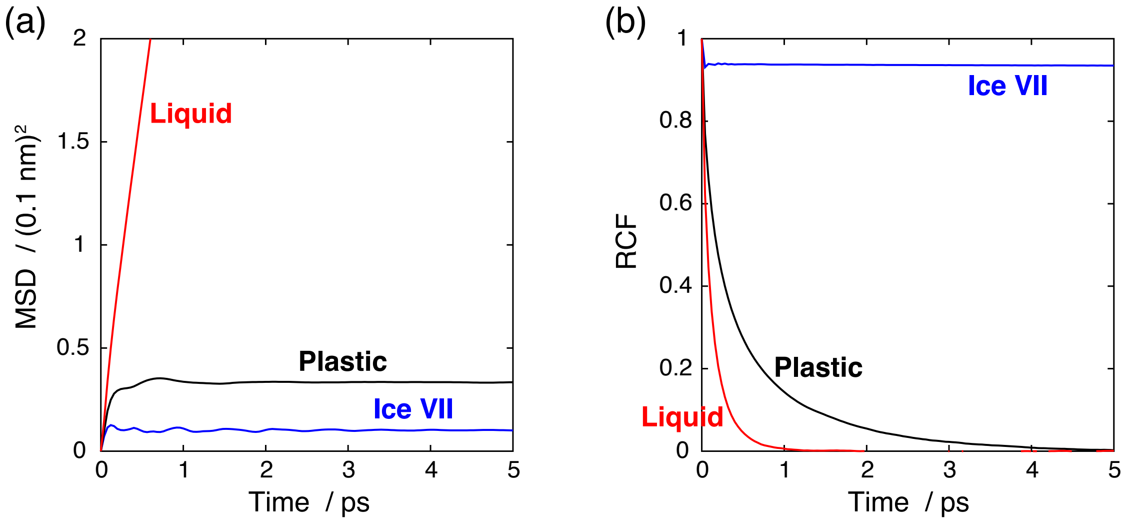

Figure 2.1

Time-correlation functions, (a) the mean square displacements and (b) the reorientational correlation functions of ice VII (500 K; blue), plastic ice (640 K; black) and liquid water (960 K; red) obtained by molecular dynamics simulations.

2.3.2 Thermodynamic and structural properties in density-adjusted quenching

In order to investigate the structural characteristics of the three phases in more detail, a direct consequence due to the density difference is removed by a simple scaling of the coordinates of water molecules; the cell size at a given instant for any phase is adjusted to have the mean cell size in the plastic phase at T = 640 K. We examine various properties of the inherent structures, which are obtained by the steepest descent energy minimization. The radial distribution functions (RDFs) for the density-adjusted structure exhibit almost complete agreement with those at the original density, from which we affirm that the present analysis is justified. The potential function to describe a pair interaction for water is composed of Coulombic and Lennard-Jones (LJ) interactions. The former is the essential part of HB in the three phases and the latter plays a role to maintain identity of individual molecules. The two sorts of interactions are equally important since a compact packing and a lower cohesive energy compete at a higher pressure. The potential energies of those three phases and the individual components are tabulated in Table 2.1. The potential energy increases in both transitions from ice VII to plastic and from plastic to liquid water in I-structure. This is also true in Q-structure. One of the most remarkable differences among the three phases is the higher LJ interaction in liquid water. Liquid water has a fairly different structure from either ice VII or plastic ice. Some peaks in the ice phase are missing in liquid water or only a trace of them appears. An intriguing feature is the position of the first peak in the oxygen-oxygen RDF for liquid water; it is closer by 0.02 nm than that for ice as shown in Fig. 2.2. The higher LJ energy seems to be accounted for by this closer separation of the neighboring molecules. Thus, a lower density in liquid does not mean a uniform expansion but some vacant space that results from a randomly arranged structure of liquid water, pushes water molecules close together, which may be caused by the intense thermal motions at a high temperature. In conjunction with the potential energies listed in Table 2.1, the binding energy distributions are calculated for the individual components, which are defined by

$$x_{\mathrm{B}}(\epsilon) \equiv \left\langle \frac{1}{N} \sum_{i} \delta\Big(\sum_{j \neq i} \phi_{ij} - \epsilon \Big) \right\rangle, \tag{2.3}$$

where ϕ_{ij} stands for a pair interaction energy between two molecules i and j, and $\langle \dots \rangle$ denotes the ensemble average. As shown in Fig. 2.3, the distribution for liquid water is almost symmetric against the binding energy and is nearly Gaussian as observed in an ambient condition [18]. It is, however, asymmetric for plastic ice. The origin of this asymmetry is explained in terms of the local hydrogen bonded network later in this section.

Table 2.1

The potential energies and those for the Lennard-Jones term and the Coulombic term of ice VII, plastic ice and liquid water for I- and Q-structure.

		I-structure			Q-structure		
		Ice VII	Plastic	Liquid	Ice VII	Plastic	Liquid
Potential energy	/ kJ mol^{-1}	–39.274	–24.705	–6.5635	–50.751	–45.283	–41.776
LJ term	/ kJ mol^{-1}	18.289	23.380	39.750	13.526	18.181	27.778
Coulombic term	/ kJ mol^{-1}	–57.563	–48.086	–46.313	–64.277	–63.465	–69.554

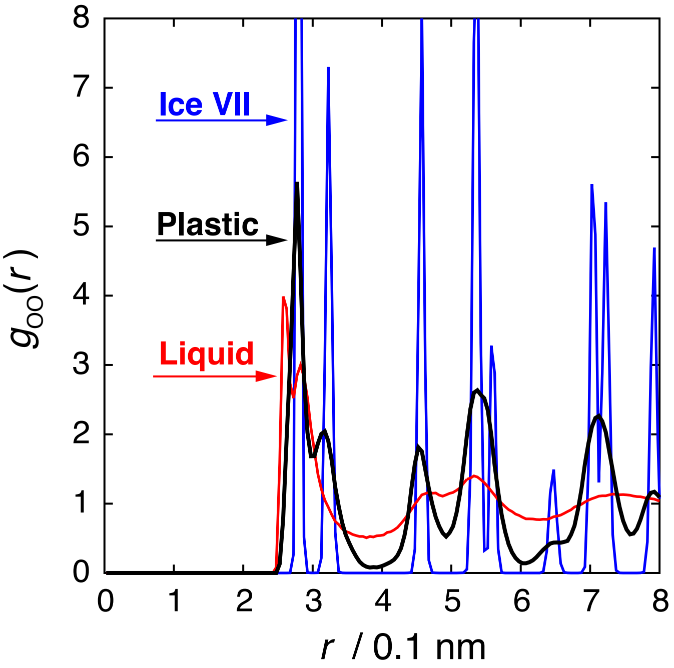

Figure 2.2

Oxygen-oxygen radial distribution functions of ice VII (blue), plastic ice (black) and liquid water (red) for Q-structure.

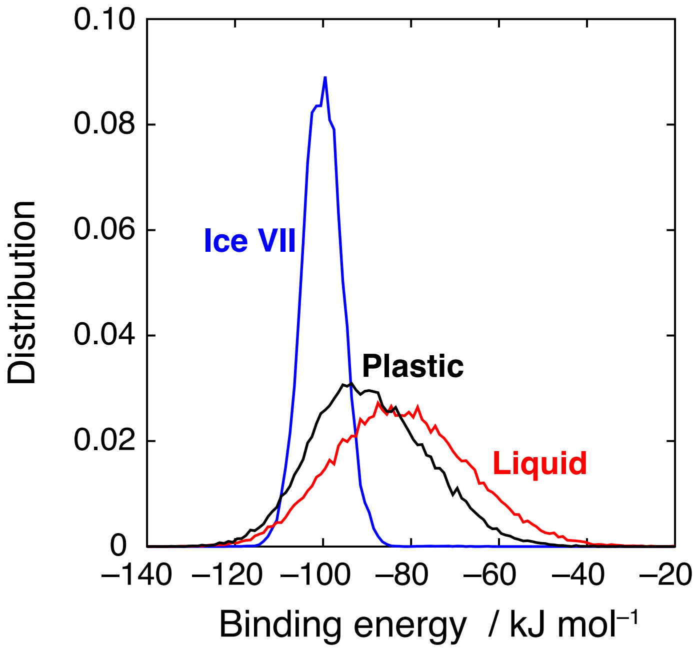

Figure 2.3

Binding energy distributions of ice VII (blue), plastic ice (black) and liquid water (red) for Q-structure.

The structure of the plastic phase is characterized by the existence of several peaks in the oxygen-oxygen RDF whose positions are the same as those in ice VII as shown in Fig. 2.2. The ratio of the second peak position to the first one is around 1.16, which indicates that both phases have a BCC lattice structure. Since the water molecules in the plastic phase are fixed in principle to the lattice position in the same way as in ice VII, the LJ term for plastic ice in Table 2.1 should have a similar value to that for ice VII. In reality, however, it is fairly higher than that for ice VII. This could be caused by small but distinct deviation of molecules from the corresponding ideal lattice sites. Indeed, the peaks in the RDF for plastic ice are blurred. Therefore, the deviation from the ideal lattice sites is examined for both ice VII and plastic ice in Q-structure. The distribution of the dislocation is Gaussian whose standard deviation is 4.5×10^{-4} nm for ice VII and is 2.7×10^{-2} nm for plastic ice. This indicates that a deviation whose magnitude is similar to the mean deviation in plastic ice cannot be observed in ice VII. Therefore, plastic ice seems to be not a variant of the ice VII form where only a small number of structural defects leaving molecules away from the lattice sites are embedded but a phase where a large number of dislocations are implemented by the Gaussian distribution with the large standard deviation. (We examine this issue in the later subsec.) The large deviation, i.e., dislocation of molecules, is associated with the higher LJ interaction energy because of the asymmetric nature of the LJ potential in the molecular separation. While the extension of the molecular separation by 0.027 nm results in a decrease in LJ energy by 4.4 kJ mol^{-1} for an ideal neighboring distance in the BCC lattice, 0.267 nm, a contraction by the same amount gives rise to an increase by 18.6 kJ mol^{-1}. Thus, the dislocation accounts for the higher LJ energy in plastic ice. The higher energy in LJ interaction is also consistent with the pair interaction energy distribution for the LJ term shown in Fig. 2.4, which is defined by

$$x_{\mathrm{P}}(\epsilon) \equiv \left\langle \frac{1}{N} \sum_i \sum_{j \neq i} \delta(\phi_{ij} - \epsilon) \right\rangle, \tag{2.4}$$

where ϕ_{ij} stands for a pair interaction energy between two moledules i and j (here for the LJ term). The pronounced peak associated with the nearest neighbors in ice VII is smeared out in plastic ice. The actual dilatation of plastic ice compared with ice VII can also be associated to the large dislocation. The difference between plastic and crystalline in simple quenching at constant volume is a little smaller in accordance with the dilatation upon transition to the plastic phase. A more detailed scrutiny of the local environment of those three phases seems to be essential in order to provide a microscopic picture of plastic ice. This is achieved from two view points; local energetic and structural aspects are examined and those are combined with the global network structure. Local structures of water and ice are described by simply the coordination number of individual molecules, which is defined by the number of molecules around a tagged molecule. An alternative expression of it is given by

$$n(r_{\mathrm{c}}) = 4\pi\rho \int_0^{r_{\mathrm{c}}} g_{\mathrm{OO}}(r) r^2 \mathrm{d}r, \tag{2.5}$$

where ρ is the average number density of the system. The upper bound of the integration, r_{c}, is usually considered to be the distance at the first minimum of an oxygen-oxygen RDF, $g_{\mathrm{OO}}(r)$. Since the cell size is adjusted to have the density of the plastic ice, it is natural to adopt the common r_{c} value, $r_{\mathrm{c}} = 0.306$ nm (the first minimum for plastic), to the three phases. The coordination distributions are shown in Fig. 2.5. The crystalline phase (ice VII) has only 8-coordinated molecules. In the plastic phase the 8-coordinated molecule is also the most dominant species but other species than the 8-coordinated one appear. The coordination number distribution in liquid is widespread with its center at 9. Especially, the populations of extremely small and large coordination number species increase in the liquid state. The average coordination numbers are 8.40 for plastic and 8.55 for liquid.

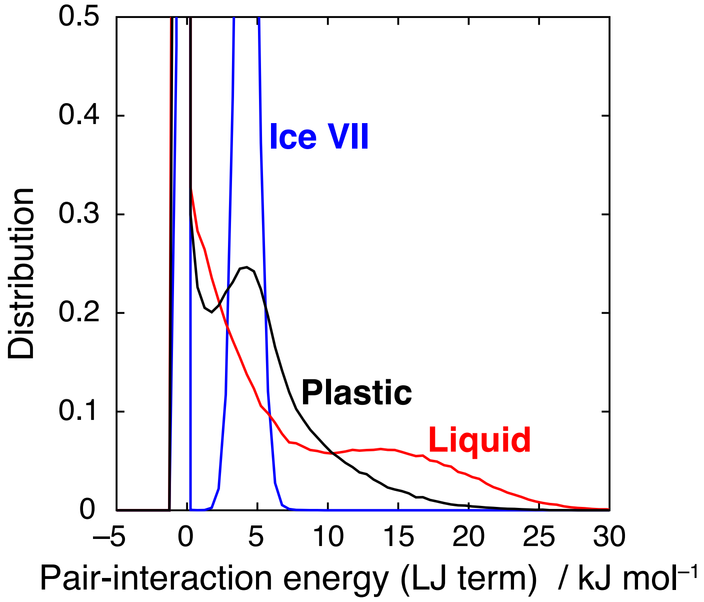

Figure 2.4

Pair interaction energy distributions for the LJ term of ice VII (blue), plastic ice (black) and liquid water (red) for Q-structure.

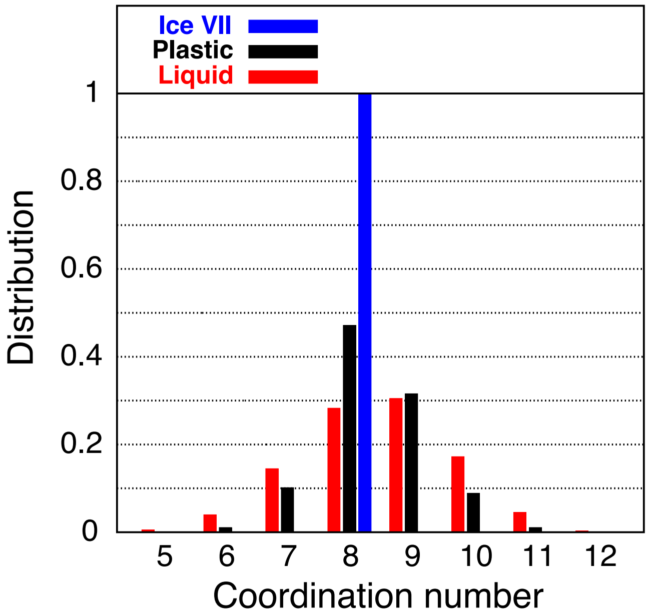

Figure 2.5

Coordination distributions of ice VII (blue), plastic ice (black) and liquid water (red) for Q-structure.

The energetic contribution to the local structure competes with the packing efficiency at a high density, a local energetic feature is represented by an HB number distribution, a distribution in which a tagged molecule has a specific number of HBs with other molecules. The HB is defined by the geometric restriction on a pair of neighboring molecules where the OH distance for the pair is smaller than 0.22 nm and the angle between the OH bond of one molecule and the direction toward the adjacent oxygen is less than $\pi/6$ (this HB criterion is almost equivalent to a certain threshold for a pair interaction energy). With this criterion we obtain the lifetimes of hydrogen bonds of those three phases. In ice VII a hydrogen bond is almost completely retained, which is consistent with the reorientational correlation in Fig. 2.1. In both liquid and plastic phases, a hydrogen bond decays in the same order as the relaxation time of the corresponding reorientational correlations. In the plastic phase, however, a hydrogen bond is almost always reformed in later time. Ice VII is composed of only molecules hydrogen-bonded with 4 neighbors but plastic ice has a wider distribution in HB number centered at 4 as shown in Fig. 2.6. In the liquid phase, a much wider one is observed and there are many defects in HB. The larger coordination number but the smaller number of hydrogen-bonded neighbors in liquid and plastic phases result in the higher potential energy than that in ice VII, since the small separation of two water molecules gives rise to the repulsive interaction without hydrogen-bonding.

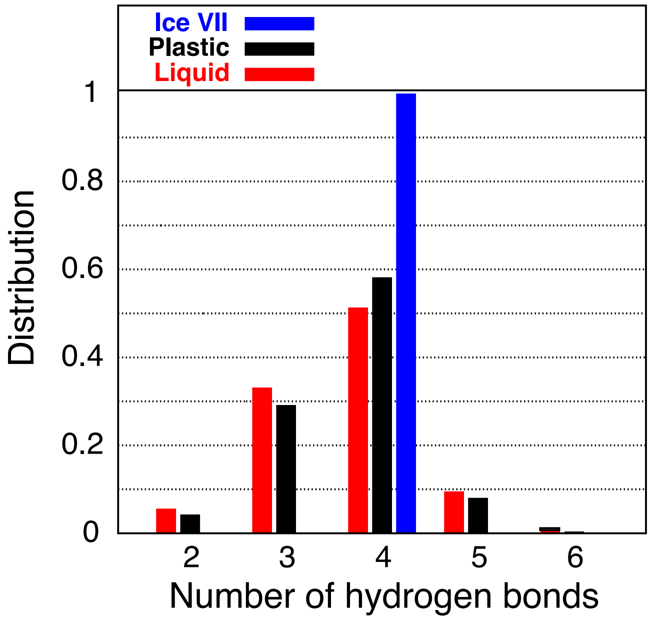

Figure 2.6

Hydrogen-bond number distributions of ice VII (blue), plastic ice (black) and liquid water (red) for Q-structure.

Liquid water has the highest LJ energy and the lowest Coulombic energy in Q-structure as in Table 2.1. The high LJ energy is associated with the closest separation of neighboring pairs as mentioned above. The low Coulombic energy in liquid water is consistently explained by the smaller molecular separation, which seems to dominate unfavorable orientations. This is confirmed by the pair interaction distributions for Coulombic energy depicted in Fig. 2.7, which is defined by Eq. 2.4 for the Coulombic term. A low energy (strong interaction) region in liquid water is a little larger, which originates from the smaller OH distance for a neighboring pair as seen from oxygen-hydrogen RDFs (Fig. 2.8).

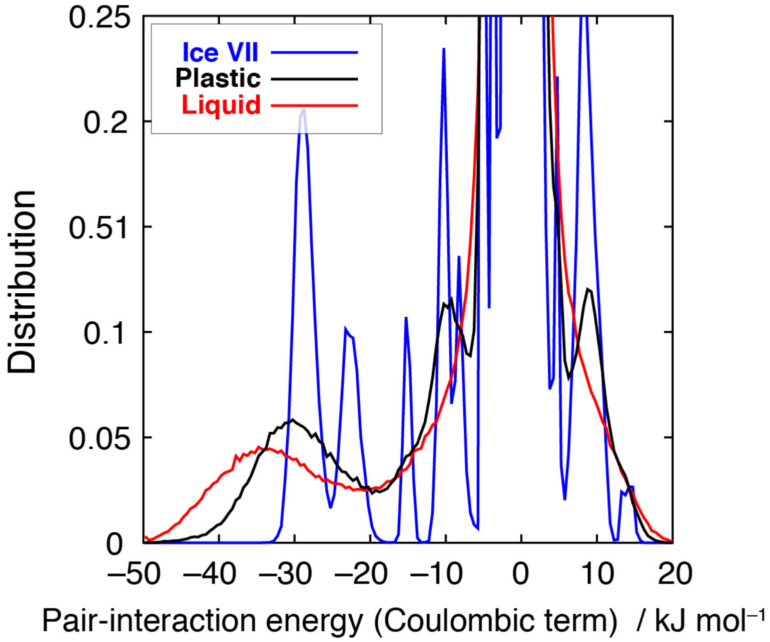

Figure 2.7

Pair interaction distributions for Coulombic energy of ice VII (blue), plastic ice (black) and liquid water (red) for Q-structure.

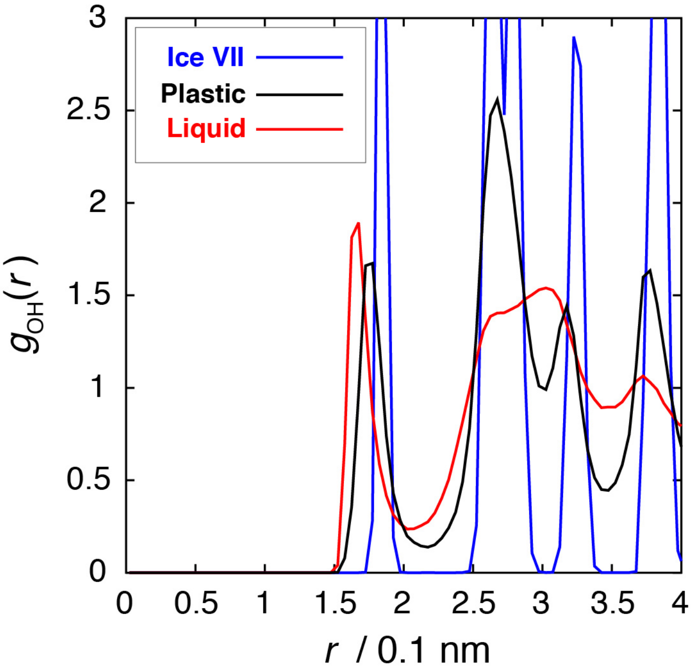

Figure 2.8

Oxygen-hydrogen radial distribution functions of ice VII (blue), plastic ice (black) and liquid water (red) for Q-structure.

2.3.3 Local hydrogen-bond network in plastic ice

Ice VII is made up of the two interpenetrating ice I*c* lattice structures. Here we call individual sublattices A and B. Any water molecule on sublattice A in ice VII forms no HB with any molecule on sublattice B. Since all the water molecules sit on the lattice sites in plastic ice, each water molecule can be classified by its location on the lattice site; called either A or B in the same way as in ice VII. Some HBs may bridge A and B sublattices by orientational defect in plastic ice. Then, a global hydrogen bond network is disrupted. It is of great interest to explore the local hydrogen bond patterns that exist in Q-structure of plastic ice.

We search for various hydrogen bond patterns in a unit cell, which contains one molecule at the center and 8 at the vertexes of the cubic box. The five most popular patterns are picked up, which are designated as type-(a) to type-(e) found in Q-structure of plastic ice. In ice VII, four of the eight vertexes in tetrahedral positions belong to the sublattice A hydrogen-bonded with the center and the sublattice B comprises the remaining four forming no HB with the center. The unique pattern observed in ice VII is type-(a) shown in Fig. 2.9(a) where all the HBs are oriented correctly to the four vertexes of the sublattice A ("right" HBs) as depicted by yellow lines in Fig. 2.9. This pattern is the most popular one even in plastic ice. The others suffer from the lack of HB and/or from orientational faults containing "wrong" HBs marked by green lines. Type-(b) has one wrong HB out of its four HBs, which orients toward one of the vertexes of the sublattice B. This is a bridging molecule disturbing a nominal HB network by combining the two sublattices. One of the four HBs is missing but the remaining three are right HBs oriented correctly in type-(c). Type-(d) contains the same number of HBs as type-(c) but one of them is a wrong HB. All three HB partners are clustered on one side of the cell as shown in Fig. 2.9(d). There is an extra (necessarily wrong) HB in type-(e) with four right HBs. The occurrence of those patterns is 28%, 21%, 13%, 9%, and 5% for type-(a) to type-(e), respectively. Each molecule at the center has a different energy and therefore occurrence of those patterns in the local connectivity seems to lead to asymmetry in the binding energy distributions for plastic ice. The Coulombic binding energy distribution of the central molecule for each type is shown in Fig. 2.10. Type-(a) has a slightly lower energy than type-(b), which originates from the functional form of the pair potential; the most favorable directions are those heading to the tetrahedrally oriented protons and lone-pairs. Type-(e) has the lowest energy among the five types due to its five HBs although one of the HBs may be a little weaker than that in type-(a) by about a few kJ mol^{-1}. This weaker HB is consistent with the higher energy in type-(b) compared with type-(a). In contrast to the observation on the existence of one wrong HB, the energy in type-(d) is lower than in type-(c). Since three HB sites in type-(d) are biased spatially, there might be some possibility for another molecule to interact with intermediate strength. The other patterns are collected to one group in Fig. 2.10.

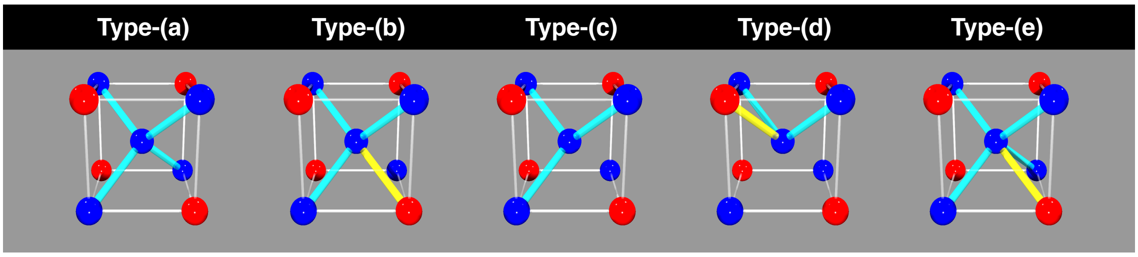

Figure 2.9

The five most popular hydrogen-bonding patterns in plastic ice at 12 GPa and 640 K. Spheres denote oxygen, which are divided into two subluttices, A and B, by colors blue and red. Blue and yellow cylinders correspond to the hydrogen bonds, which connects water molecules on the same sublattice and bridges different sublattices, respectively. Hydrogen atoms are not illustrated.

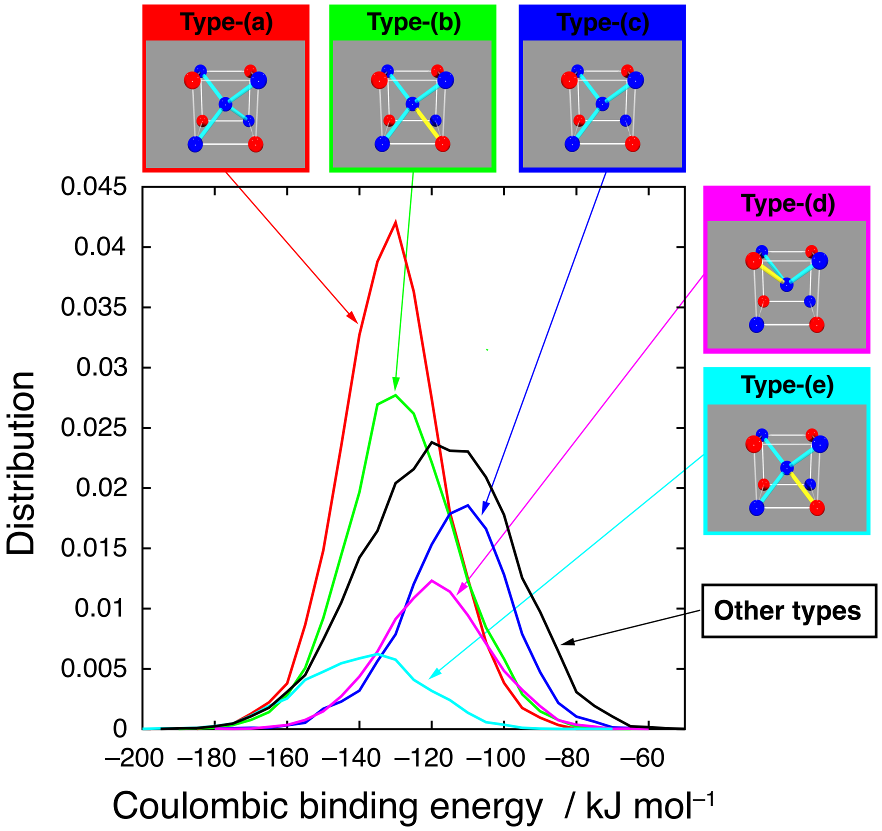

Figure 2.10

Coulombic binding energy distributions of the central molecule for type-(a) to (e) and in other types.

Considering fairly high occurrences of type-(c) and (d) as well as the patterns other than (a) to (e), they are responsible for the asymmetry in the binding energy distribution in plastic ice. There are a large amount of hydrogen-bonds which do not orient to the tetrahedral directions such as type-(b), (d), and (e). Frequent occurrence of these patterns leads to fusion of the two sublattices rather than defect-containing ice VII. It is noted that there are a large amount of unit cells with orientational (HB) defects. Each sublattice may not be connected by way of the unit cells having perfect local orientation, i.e., type-(a). In fact, the site-percolation threshold for the diamond structure is known to be 0.43, which is much higher than the occurrence of type-(a), 0.28 [38,39].

2.4 Conclusion

In the present study, the properties of the plastic ice phase are elucidated by the potential energy distributions decomposed into the Coulombic and LJ interactions and by classification of the local structures. In comparison with liquid water and ice VII in density-adjusted I- and Q-structure, the following three characteristics of the plastic ice phase are found.

Firstly, the LJ interaction in the plastic phase is found to be more repulsive than that in ice VII even though water molecules are placed on the BCC lattice sites in both phases. In the plastic phase the water molecules rotate at the cost of potential energy in order to acquire rotational entropy, which is estimated to be about 12 J K^{-1} mol^{-1}. This value is to be compared with 5 J K^{-1} mol^{-1} for the translational one at the melting from plastic ice to liquid water. A large amount of HBs are broken due to the thermal motions at high temperatures and the hydrogen bond connectivity of water molecules is fairly disturbed, which causes the dislocation of the molecules in the plastic phase from their ideal lattice points.

Secondly, Coulombic interaction in liquid water is stronger than that of any other phase. In crystalline solid, the positions of molecules are fixed around the lattice points and the Coulombic interaction is well balanced with the LJ repulsion. In liquid water, on the contrary, a pair of water molecules can be close together, say, within 0.25 nm. This short distance brings the stronger LJ repulsion but it is compensated with the stronger Coulombic attraction.

Finally, we have focused on the asymmetric distribution in the Coulombic binding energy of plastic ice. The main peak of the distribution is contributed from the water molecules having four regular hydrogen bonds with surrounding molecules while the shoulder comes from the disordered local structures, which have only three hydrogen bonds. More than half of the water molecules have a HB bridging the two sublattices.

Thus the sublattices of ice VII are fused in the plastic ice.

Chapter 3

Rotational dynamics of plastic ice

The work here focuses on the dynamics of the water molecules in the phases at high temperature and pressure, i.e., ice VII, plastic ice, and liquid water. The hydrogen-bond correlation function providing the lifetime of hydrogen bonds is compared to the reorientational correlation function to examine a relation between a rotation of an individual molecule and an energetic relaxation process. The hydrogen-bond correlation function of plastic ice decays in a way similar to liquid but it converges to a finite value as seen in ice VII, reflecting the rotational motion of the water molecule at the fixed location. In addition, the relaxation times of the two correlation functions for plastic ice resemble one another, confirming the fact that only the rotational motion invokes the hydrogen-bond rearrangements in plastic ice.

3.1 Introduction

Water is the most ubiquitous substance on the earth and is indispensable for biological systems. While a water molecule is simple, water exhibits various versatilities and anomalies, that is, diversity of the condensed phases. In fact, the number of crystalline structures exceeds 16 according to experimental investigations and theoretical predictions as of the present time [2,24–26]. In addition, the most unique feature in condensed phase is its polyamorphism, which may be associated with the other anomalies in supercooled liquid state [40].

The existence of the plastic phase (plastic ice) —— the almost free rotational phase with no molecular diffusion —— has been predicted by computer simulation, as one of the new stable states of water in high pressure region [13,16,41]. Plastic ice intervenes between ice VII and the supercritical fluid water as the two lattice types: one is the body-centered cubic (BCC) lattice and the other is the face-centered cubic (FCC) one. The BCC-type plastic ice exists under lower pressure while the FCC-type one does un- der higher pressure. The various properties of plastic ice have been elucidated in Refs. [13] and [16]. Ref. [16] poses an extended phase diagram of water including the plastic phase. There are, however, unexplained structural and dynamic properties of plastic ice.

In the present work, we analyze the rotational dynamics of ice VII, plastic ice, and liquid water at high temperature and pressure in order to elucidate the characteristics of the dynamics in plastic ice. The reorientational correlation function and the HB correlation function are calculated from the simulation results and the characteristic relaxation time of liquid water and plastic ice are examined.

3.2 Methods

In order to scrutinize the HB dynamics in plastic phase by comparing it with two other phases, three representative states are chosen at a fixed pressure of 12 GPa. Those correspond to crystalline ice VII, plastic structure, and liquid water, which are obtained at $T = 500, 640$, and 960 K. Molecular dynamics simulations are performed for longer time than 8 ns with an initial ice VII structure. The temperature and pressure are fixed by Nosé-Andersen thermo-barostat [42–44]. A simple periodic boundary condition is applied to a cubic box containing 432 water molecules. Water-water interaction is described by the TIP5P potential, which is made of two protons each with a positive fractional charge, two negative charge sites, and an oxygen nucleus interacting with Lennard-Jones potential [22]. The resultant densities of ice VII, plastic ice, and liquid water turn out to be 1.8703, 1.7699, and 1.6393 g cm^{-3}, respectively.

3.3 Results and discussion

3.3.1 Mean square displacement and reorientational correlation function

In Fig. 2.1 in Chapter 2, I showed the mean square displacement (MSD) defined by Eq. 2.1 and the reorientational correlation function (RCF) defined by Eq. 2.2. In ice VII, individual molecules stay at the original positions and that the MSD of ice is constant after a short rise period caused by vibrational motions. The RCF is also constant, with an initial decay to 0.95 due to the librational motions. In liquid water, on the other hand, the MSD increases linearly with time and orientational correlations are lost within 1 ps after a rapid decrease by the librational motions. Plastic ice behaves similarly to crystalline ice in translational motion with a larger amplitude of vibrations while its rotational motion is a close analogue of liquid. The ice-like MSD indicates the nondiffusional molecular motion in the plastic phase. Random rotations of the molecules can also be identified by the convergence toward 0 of the RCF [41]. Relaxation time of rotation is discussed in subsection 3.3.3.

3.3.2 Hydrogen bond correlation

Individual water molecule in the liquid and the plastic phases makes rapid and incessant rotational motions, which inevitably induce the rearrangements of HB network structure. While, the way of the alternation and the lifetime of the HB depends on the phase. It is therefore intriguing to examine the HB time correlation which may feature the possible partners of HBs as well as the HB lifetime. In order to shed a light on these properties, we adopt a history-independent correlation function of HB [45]. It is given as

$$c_{\mathrm{HB}}(t) \equiv \frac{\langle \delta h_{ij}(0)\delta h_{ij}(t)\rangle}{\langle [\delta h_{ij}(0)]^2\rangle}, \tag{3.1}$$

where $h_{ij}(t)$ is a binary function defined as $h_{ij}(t) = 1$ if a pair of water molecules i and j are hydrogen-bonded, and $h_{ij}(t) = 0$ otherwise, and $\delta h_{ij}(t) \equiv h_{ij}(t) - \langle h\rangle$. The angular bracket indicates an average over all the pair of molecules and the time origin. In the infinite system, $\langle h\rangle$ is zero and that the formula is written in much simpler form. The averaged number of HBs per water molecule, say n_{HB}, is defined as

$$n_{\mathrm{HB}} = (N-1)\langle h\rangle. \tag{3.2}$$

A hydrogen bond is defined according to the mutual geometry of a pair of molecules; the distance between an O atom on one molecule and a proton on another molecule is less than 0.22 nm and the angle for a vector connecting two oxygen nuclei and the OH arm is within ±30° [41].

$c_{\mathrm{HB}}(t)$ indicates a probability of finding a hydrogen bond at the molecular pair i and j which are hydrogen-bonded at time $t = 0$. Decay of c_{HB} characterizes the lifetime of the bond. $c_{\mathrm{HB}}(t)$ converges to the different values in the different phases reflecting the HB network rearrangement dynamics. In the liquid phase, $c_{\mathrm{HB}}(t)$ converges to zero. This is because the hydrogen-bonded pair at $t = 0$ breaks off its adjacency after a long time by molecular displacements. In ice, on the other hand, c_{HB} remains to be around unity after a long time, because all the HBs are maintained except the case when they are broken by thermal vibrations with probability q. c_{HB} is then expected to converge to $(1-q)$ in a large system. In the plastic phase, HB rearrangements are allowed but the molecules cannot be dislocated from the initial position. The bond initially connected will be connected again with a certain probability after a long time. In such a case, c_{HB} remains finite. c_{HB} is expected to converge to $p = n_{\mathrm{HB}}/n_{\mathrm{c}}$ in a large system, where n_{c} is the coordination number. Here n_{HB} in the plastic phase is 3.08 and if n_{c} is ideally set to be 8 (the number of neighbors per molecule in BCC lattice), the expected asymptotic value is 0.385.

Figure 3.1 shows that $c_{\mathrm{HB}}(t)$ in liquid eventually decays to 0. This behavior is roughly similar to that in the RCF. This suggests that a HB cleavage is mainly dominated by rotational motion of an individual molecule. Convergence to zero is, however, realized by additional diffusional motion. A very fast initial decay of $c_{\mathrm{HB}}(t)$ for ice VII is also observed in the reorientational correlation function and therefore this decay is associated with the librational motions. A more interesting decay is indeed obtained for $c_{\mathrm{HB}}(t)$ for the plastic phase. A hydrogen bond once formed in plastic ice exhibits a decay similar to liquid water. However, an asymptotic behavior is different. $c_{\mathrm{HB}}(t)$ converges to a finite value, 0.323, indicating the recurrence of the HBs. Thus, it is another evidence that water molecules rotate but do not translate diffusively.

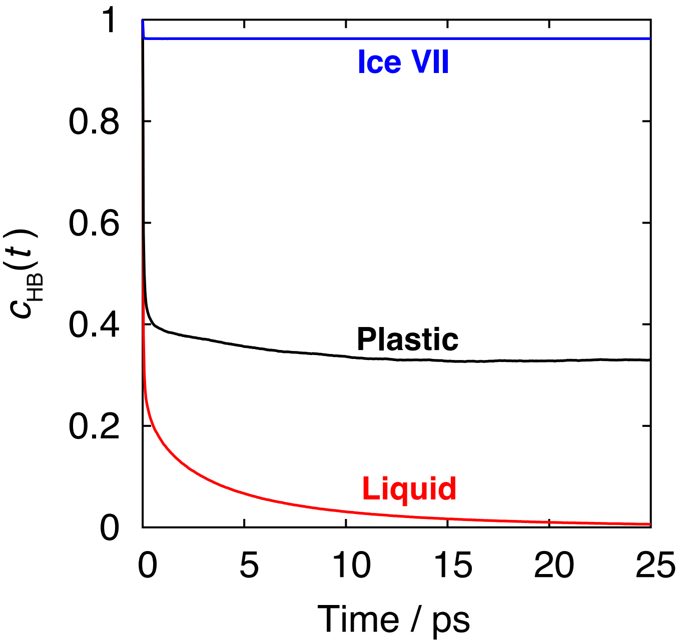

Figure 3.1

The hydrogen bond correlation functions of the three phases against time. Blue, black, and red correspond to ice VII, plastic ice, and supercritical fluid water, respectively.

3.3.3 Relaxations of reorientational and hydrogen-bond correlations

Figure 3.2 shows the short-time behaviors of the reorientational and the HB correlation functions for the plastic and the liquid phases. After the initial very fast decay corresponding to the librational motions, a linear decay is observed. The relaxation times for the reorientational and the HB correlation functions of the plastic and the liquid phases are listed in Table 3.1.

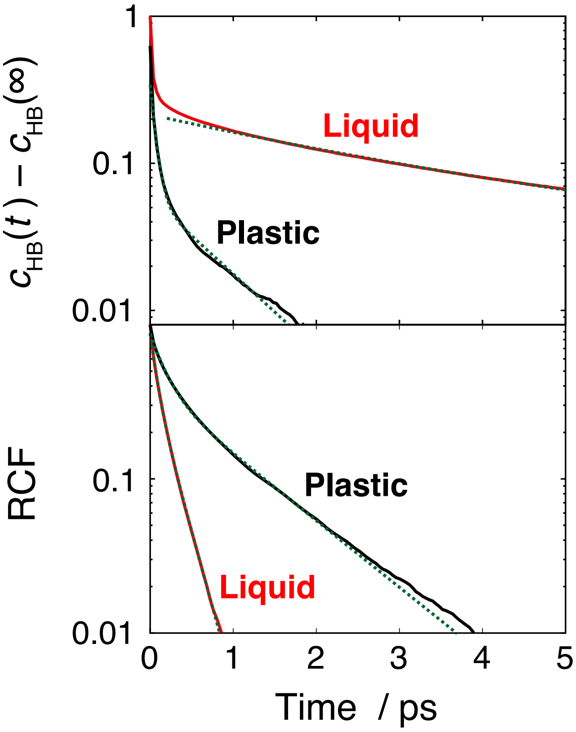

Figure 3.2

Reorientational and HB correlation functions plotted against time in lower and upper panels, respectively. Red and black lines indicate the liquid and the plastic phases, respectively. Dashed lines are approximations with the sum of two exponential functions.

Table 3.1

Relaxation times of various correlation functions in the units of pico-second.

	Reorientational	Hydrogen bond
Plastic	1.01	0.839
Liquid	0.223	2.54

The clearest characteristic in Fig. 3.2 and Table 3.1 indicates the relevance of the slopes (relaxation times) between the plastic and the liquid phases in the RCF and the c_{HB}. That is, the RCF of liquid water has a shorter relaxation time than that of plastic ice, reflecting the temperature difference in both phases, while the relaxation time of c_{HB} for liquid is much longer than that for plastic ice. To elucidate the origin of the discrepancy, they are compared from the different aspect. The relaxation time of plastic ice is similar in the both correlation functions, and also close to those of liquid water at ambient condition [45,46]. Since each water molecule in plastic ice rotates at a fixed location and that the $c_{\mathrm{HB}}(t)$ depends mainly on the rotational motion, both the RCF and the c_{HB} of plastic ice decay similarly. A prominent difference is found in the relaxation times of the two correlation functions of liquid water where c_{HB} decays much slower than the RCF. In order to explain it, we focus on the liquid water's relaxation time of c_{HB}, 2.54 ps. The MSD at time $t = 2.54$ ps is about 7.8 Å^2, i.e., the deviation from the position at time origin is 2.8 Å on average. This distance corresponds to the distance between nearest-neighbor water molecules at the present pressure and temperature [13]. Displacement of the water molecules from the initial location provokes the permanent dissociation of the hydrogen-bonded pairs. Thus the relaxation time can be considered as the lifetime of HBs induced by molecular translations.

Debye-Stokes-Einstein relation [47] relates the rotational relaxation time τ_1 with viscosity η by $\tau_1 = 4\pi\eta R^3/k_{\mathrm{B}}T$, where R is the hydrodynamic radius of the reorienting molecules, k_{B} the Boltzmann's constant, and T the temperature. It denotes that the relaxation time is proportional to the viscosity and the inverse temperature. Rotational relaxation time of HDO at ambient condition is 2.5 ps to 3.0 ps [46,48] and that of H_2O should be shorter owing to its smaller moment of inertia. The viscosity η of water at 960 K and 12 GPa is comparable to that at ambient condition [49]. By taking them into consideration, the rotational relaxation time of liquid water at 960 K and 12 GPa is estimated to 0.5 ps, which is in quite a good agreement with our calculation result.

There is no information available for the HB lifetime of the supercritical fluid water at high pressure, but Petrenko *et al.* showed by computer simulation using TIP4P-HB model that the HB lifetime of the supercritical water depends only on density and is independent from temperature [50]. Their plot suggests the HB lifetime at the present density will be longer than 2 ps, which is in good agreement with our result.

Molecular dynamics simulations with SPC/E water model elucidates that the HB lifetime of water at ambient condition is comparable to the reorientational relaxation time [45,51]. In our results at high temperature and pressure, on the other hand, they differ about one order of magnitude, suggesting that the mechanism of the HB rearrangements at high temperature and pressure, namely supercritical fluid water, is different from normal liquid water. Further analyses are awaited. The relaxation times for plastic ice are verifiable by the ultrafast infrared spectroscopy [46,48].

3.4 Concluding remarks

In this paper, we discuss the reorientational dynamics of water molecules in plastic ice, ice VII, and liquid water at high temperature and pressure. The HB correlation function in plastic ice exhibits the intermediate behavior between ice VII and liquid state. That correlation decays like liquid but it converges to a finite value like ice VII, reflecting the rotational motion of a water molecule at a fixed location. It is found that the relaxation time of the HB correlation function is much longer than that of the reorientational correlation function for liquid water at high temperature and pressure, while the relaxation times of the two correlation functions for plastic ice are comparable. This is probably because only rotational motion invokes HB rearrangements in plastic ice while a translational motion is coupled in liquid water giving a rise to an HB relaxation.

It should be noted that discussion and conclusion in this paper are essentially independent from the HB definitions. We also investigate HB correlations employing another major HB definition according to the pair interaction energy, in which two water molecules are regarded to be hydrogen-bonded if the pair interaction is lower than -16 kJ mol^{-1}. In fact, qualitative features in HB decay are found to be insensitive to the definition of HB.

Chapter 4

Yet another criticality of water

A phase behavior around the transition between ice VII and a plastic phase of water is investigated by molecular dynamics simulation and the subsequent analysis on the basis of Landau theory. The prior works have predicted that the phase transition between ice VII and plastic ice is a first-order transition on the ground of a weak hysteresis and so on. Rigorous survey in the present report, however, augments their prediction with new evidences that a first-order phase transition line gives way to a second-order one at higher pressures, where a tricritical point joins these phase boundaries together. Critical phenomena are also observed whereby, other than that associated with the hypothetical critical point in the deeply supercooled state, which could influence the physical properties in a wide range of temperature and pressure. A new critical behavior is affirmed by the result that the scaling law holds at any pressure on the second-order phase transition line for which the critical exponents are estimated. We introduce an appropriate order parameter to obtain the Landau free energy functional and the change in the functional against temperature accounts for the phase behaviors. This also enables to estimate the coexistence and the spinodal lines at pressures below the tricritical point, all of which compensate those obtained directly by molecular dynamics simulations. These results allow us to anticipate that the critical fluctuations may give us clue for determining the phase boundary experimentally.

4.1 Introduction

Water has at least 16 crystalline polymorphs including metastable states and a non-molecular solid [1]. Almost all the polymorphs do not occur on Earth but surely distribute at many places inside and outside the solar system, and often play crucial roles in the planetary geology [52]. Among the molecular crystalline phases, ice VII is one of the densest ices and also occupies the widest area on the pressure-temperature plane. Each polymorph of water has its mystery, and so does ice VII. Melting curve of ice VII to high-pressure liquid water has not been settled by experiments [3–10]. We have proposed the intervention of a plastic phase of ice (plastic ice) between ice VII and liquid water based on molecular dynamics (MD) simulations and the free energy calculations [13], which enables to account for large gaps among various experimental curves of ice VII [13,15,16]. In plastic ice, water molecules are fixed at the lattice points while they rotate freely [13,15,16,41].

The phase transition between ice VII and plastic ice is reported to be first-order on the basis of i) appearance of small hysteresis in the forward and backward transition between them; and ii) the slopes of two free energy curves at the intersection [13,15,16]. On the other hand, owing to the proton disorder in ice VII, its structure already acquires a high symmetry and the transition to plastic ice accompanies only a minor symmetry change. Thus it can be a kind of order-disorder phase transition of either first- or second-order [53]. The transition, therefore, deserves a close scrutiny.

Much attention has been paid to the critical phenomena of water. Critical phenomena are spectacular collective ones accompanying the divergent character in fluctuations in both time and space. In addition to the trivial vapor-liquid critical point, water is conjectured to possess the second (metastable) critical point. It will terminate the coexistence line between two different liquid states of water in the supercooled region of the metastable phase diagram of liquid water, and its critical fluctuations may even affect the properties of liquid water at room temperature, which is observed as the anomalies of water [54–57]. Thus the single critical point wields influences to a wide area of the phase diagram, and that is the different point from the first-order phase transitions.

In the present work, the phase behaviors are reexamined in more detail using TIP5P-E water model [23]. It is found that the behaviors are fairly complicated, that is, a first-order phase transition ("coexistence") line gives way to a second-order ("critical") one at higher pressures, where a tricritical point joins the boundaries together at around 13.3 GPa. A further analysis is made according to the Landau theory with an appropriate order parameter as explained below. We estimate the location of the coexistence and spinodal lines in the phase diagram by exploiting Landau free energy functional. We also estimate the critical exponents and affirm the scaling law holds well regardless of pressure. The phase boundaries, shown in Fig. 4.1(a), will be explained in detail in the following sections.

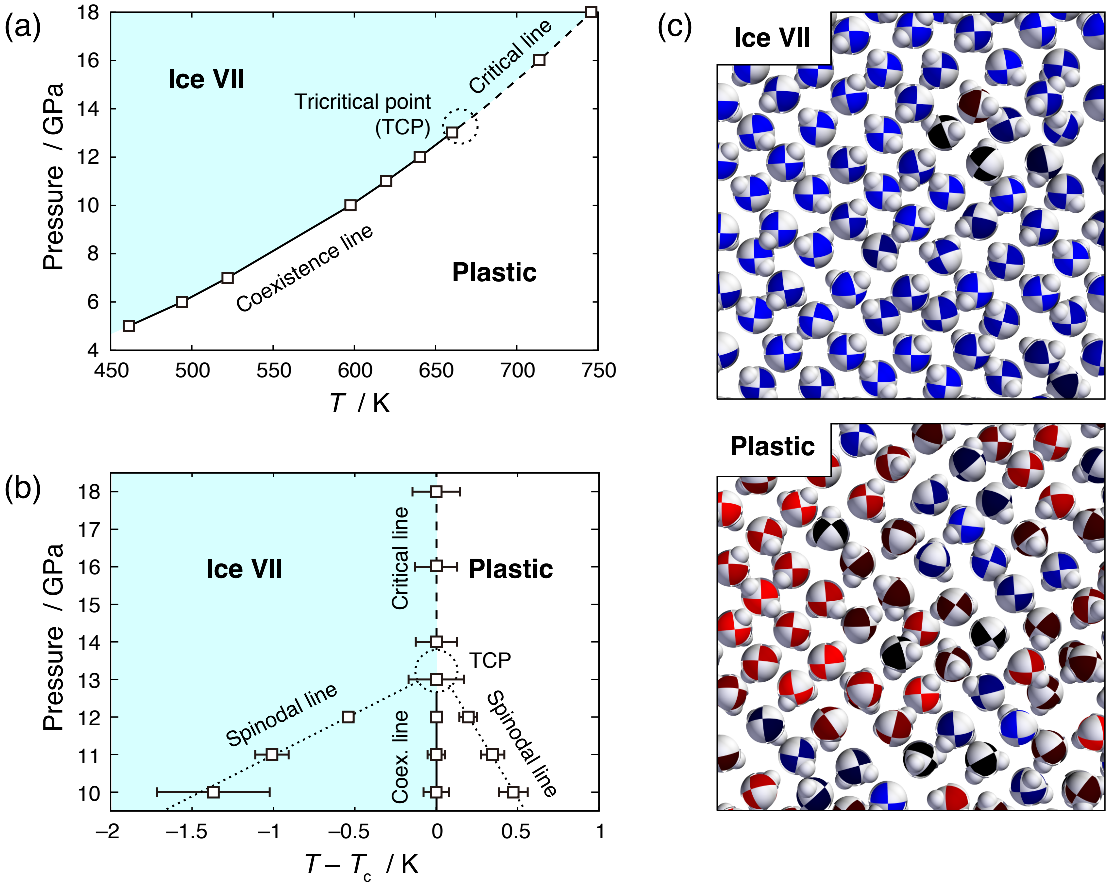

Figure 4.1 | Phase diagram of ice VII and plastic ice

(a) Phase boundaries between Ice VII and plastic ice, deduced from computer simulations. Coexistence and critical lines are plotted with solid and dashed lines, respectively. The dotted circle indicates the estimated location of the tricritical point (abbreviated as "TCP").

(b) Phase diagram plotted against the relative temperature from T_c. T_c means the coexistence temperature (at pressures below TCP) or the critical temperature (above TCP). Solid, dashed, and dotted lines are the coexistence, critical, and spinodal lines, respectively. Dotted circle indicates the estimated location of the tricritical point. Squares below 13 GPa are obtained by polynomial expansion of Landau free energy function and the remaining points are obtained by the finite-size scaling.

(c) Snapshots of ice VII at 455 K (upper) and plastic ice at 456 K (lower). Pressure is 5 GPa. Only one layer of crystal structure is cropped out. Oxygen atom is painted in chessboard pattern to clarify the molecular orientation and also gradated from red (–1) to blue (+1) according to the bond order parameter defined in Methods section.

4.2 Methods

Molecular dynamics simulation.

Ice VII is heated and plastic ice is cooled in isothermal-isobaric ensemble molecular dynamics simulation [58]. Nosé-Andersen method is used for controlling temperature and pressure [42,44]. Pressure is set to 5, 6, 7, 8, 9, 10, 11, 12, 13, 14, 16, 18, and 26 GPa. Cubic simulation cell with the periodic boundary conditions contains 1024, 2000, 3456, or 5488 water molecules. We employ the TIP5P-E rigid water model [23], whose pair potential function is represented by the sum of Lennard-Jones interaction and Coulombic interaction terms. Both interactions are truncated at 0.85 nm and the long-range interactions are corrected by analytical formula [59] for Lennard-Jones term and by a reaction-field method [23,59] for Coulombic term. Simulation time is 1 to 10 ns including 500 ps of thermal equilibration time after heating or quenching.

Hydrogen bond definition.

A hydrogen bond is defined for a pair of water molecule whose intermolecular oxygen-hydrogen distance is less than 0.22 nm [41].

Order parameter discriminating ice VII and plastic ice.

We introduce an appropriate order parameter distinguishing the essential structural difference between ice VII and plastic ice. In ice VII, all water molecules are arranged in body-centered cubic (BCC) lattice and coordinated by 8 neighbors, and each water molecule is linked to the staggered four out of 8 sites by hydrogen bonds. Note that there are two alternative ways in placing the bonds on the same BCC lattice to make up the perfect ice VII structure. Let “A” and “B” denote the twin structures. That is, a staggered half of 8 neighbors are hydrogen-bonded in twin A that are not bound in twin

B. We therefore give bond parity a_{ij} for all neighboring pairs (i, j) in a BCC lattice: a_{ij} is +1 if the neighboring pair (i, j) is hydrogen bonded in structure A and −1 otherwise. Water molecules in plastic ice are also bound to the BCC lattice points but are allowed to change their HB partners almost freely [41]. The bond order parameter for a molecule i, say ϕ_i,is defined by

$$\phi_i = \frac{1}{4}\sum_{j}^{\mathrm{NN}} a_{ij} b_{ij}, \tag{4.1}$$

where NN means the nearest 8 neighbor sites of molecule i and b_{ij} is 1 if there is a hydrogen bond between molecular pair (i, j) at a given instant and 0 otherwise. Time average of ϕ_i becomes 0 if molecules rotate freely and remains finite if the structure is fixed to either A or B of the ice VII structure. Order parameter of a system, say ϕ, is defined as the average over all molecules of the bond order parameter:

$$\phi = \frac{1}{N}\sum_{i=1}^{N} \phi_i, \tag{4.2}$$

with N being the number of molecules in the system. ϕ is +1 or −1 for perfect ice VII and 0 for plastic ice. Note that there exist water molecules that incessantly change their orientations even in ice VII by thermal fluctuation, but total flipping between the twin structures was not observed except in the vicinity of a certain thermodynamic state in our simulations. Thus the order parameter is designed to distinguish three possible states (twin ice VII and a plastic ice).

Finite-size scaling.

A finite-size scaling technique is employed for estimating the critical temperature T_c and the critical exponent ν for the correlation length of the bond order parameter [60]. We use a formulated scaling hypothesis for a physical quantity A as a function of temperature (T) and side length of system (L),

$$A(T, L) = L^{x_A/\nu} f_A(L^{1/\nu}\epsilon), \tag{4.3}$$

where x_A is the critical exponents for A, $\epsilon \equiv T/T_\mathrm{c} - 1$ is the reduced temperature, and $f_A(\cdot)$ denotes an arbitrary scaling function for quantity A.

In this work, as the physical quantity A in Eq. 4.3, we choose the Binder parameter defined as a function of the order parameter of system, $\phi \equiv \phi(T)$, by

$$B(\phi; T) \equiv \frac{1}{2}\Big(3 - \frac{\langle\phi^4\rangle}{\langle\phi^2\rangle^2}\Big). \tag{4.4}$$

The critical exponent for $B(\phi;\, T)$ is known to be zero [61], thus the Eq. 4.3 become simple: $B(T, L) = f_B\big(L^{1/\nu}\epsilon\big)$. One can get T_c and ν simultaneously in determining the regression function $f_B(\cdot)$.

4.3 Results and discussion

Our simulations present a hysteresis at and below 7 GPa in the physical quantities between heating and cooling processes (Fig. 4.2(a)). Thus the phase transition between ice VII and plastic ice is apparently first-order one. Also, the density and potential energy shown in Fig. 4.2(a) indicate that these values are system-size independent. Structural difference between ice VII and plastic ice is illustrated in Fig. 4.1(c).

At 8 GPa and higher pressures, hysteresis between heating and cooling processes disappears. Moreover, at pressures not lower than 10 GPa, a high peak in the heat capacity at constant pressure (C_p) is observed, suggesting the emergence of the critical phenomena and second-order phase transition. Interestingly, such a high peak persists even at much higher pressure, implying that the first-order phase transition line may not be terminated by the single critical point but replaced by the second-order phase transition line that continues to higher pressures.

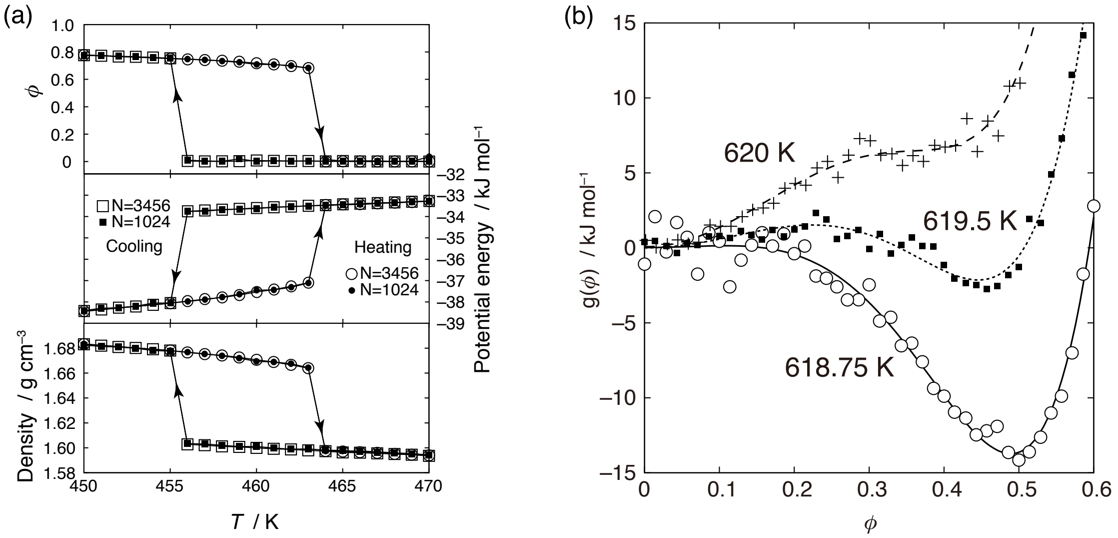

Figure 4.2 | First-order phase transition

(a) Hystereses of order parameter of system (ϕ), potential energy and density at the first-order phase transition. Pressure is 5 GPa. Open large and filled small symbols are values for systems of N=3456 and 1024, respectively, and squares and spheres are values for cooling and heating paths, respectively.

(b) Landau free energy profiles $g(\phi; T)$ plotted against ϕ. Only the right half is drawn. Three temperatures at 11 GPa are exemplified: open circles, filled squares, and crosses indicate the raw free energy curves obtained from the histogram of order parameters at 618.75, 619.5, and 620 K, respectively. Solid, dotted, and dashed lines are 6th-order even polynomial fits of them.

Here, we should examine the divergent characters with much caution. When the system size is not large enough, incessant alternations occur between states, and the first-order phase transition looks as if it were second-order. Thus, a simple time evolution of a thermodynamic property by computer simulation is not useful to discriminate whether the phase transition is first-order or second-order. In the present case, such ambiguity of phase transition arises at pressures between 8 and 13 GPa. To overcome this difficulty, we employ two different approaches: i) associating the observed transition with a phenomenological free energy ("Landau free energy") profile [62] along the appropriate transition path in order to determine the asymptotic behavior of spinodal and coexistence lines; and ii) applying finite-size scaling [60] in order to determine the critical temperatures.

The Landau free energy is defined as a function of the order parameter of system, ϕ ($\equiv\phi(T)$, defined in Methods section), by $g(\phi;\, T) = -\, kT \ln W(\phi;\, T)$, where k is Boltzmann constant, T is the temperature of system, and $W(\phi;\, T)$ is the normalized probability density that the order parameter has value between ϕ and $\phi+\mathrm{d}\phi$. Fig. 4.2(b) shows $g(\phi;\, T)$ in the positive ϕ range for several temperatures at 11 GPa. One can see $g(\phi;\, T)$ has *three minima* at an appropriate temperature, suggesting that three states can coexist if the system size is large enough. $g(\phi;\, T)$ curves are then expanded in sixth-order even polynomial functions whose minima and inflection points can be determined analytically. The coexistence and spinodal temperatures are estimated from the dependence of polynomial coefficients on the temperature. (Detailed procedure is described in Appendix for Chapter 4. See Fig. A4.1.) These enable us to estimate the first-order phase transition line extended up to 12 GPa where a direct observation of the hysteresis is difficult. Estimated coexistence and spinodal lines are listed in Table 4.1 and plotted in Fig. 4.1(b).

Table 4.1 | Coexistence and spinodal temperatures

T_c indicates coexistence temperature. T_0 and T_1 indicate lower and higher spinodal temperatures, respectively. How to determine T_c, T_0, and T_1 is described in Appendix for Chapter 4 in detail.

Pressure / GPa	T_c / K	T_0 / K	T_1 / K
12	640.28(3)	639.74(3)	640.47(6)
11	619.66(5)	618.65(1)	620.00(7)
10	597.69(8)	596.3(4)	598.16(9)
7	(522)†	517.5*	523.5*
6	(494)†	486.5*	496.5*
5	(461)†	451.5*	464.5*

* Determined by the hysteresis between cooling and heating processes.

† Interpolated from two spinodal temperatures using an approximation described in Appendix for Chapter 4.

Next, we employ a finite-size scaling technique for pressures at and above 10 GPa to examine the scaling behaviors as well as critical temperatures. At these pressures, as mentioned above and shown in Fig. 4.3(a), the peak position and height of C_p change by system size, suggesting the criticality of the finite-size system. We show the scaled heat capacities at constant pressure at 14, 16, and 18 GPa in Fig. 4.3(b), which indicate the scalability of the quantity against the system size.

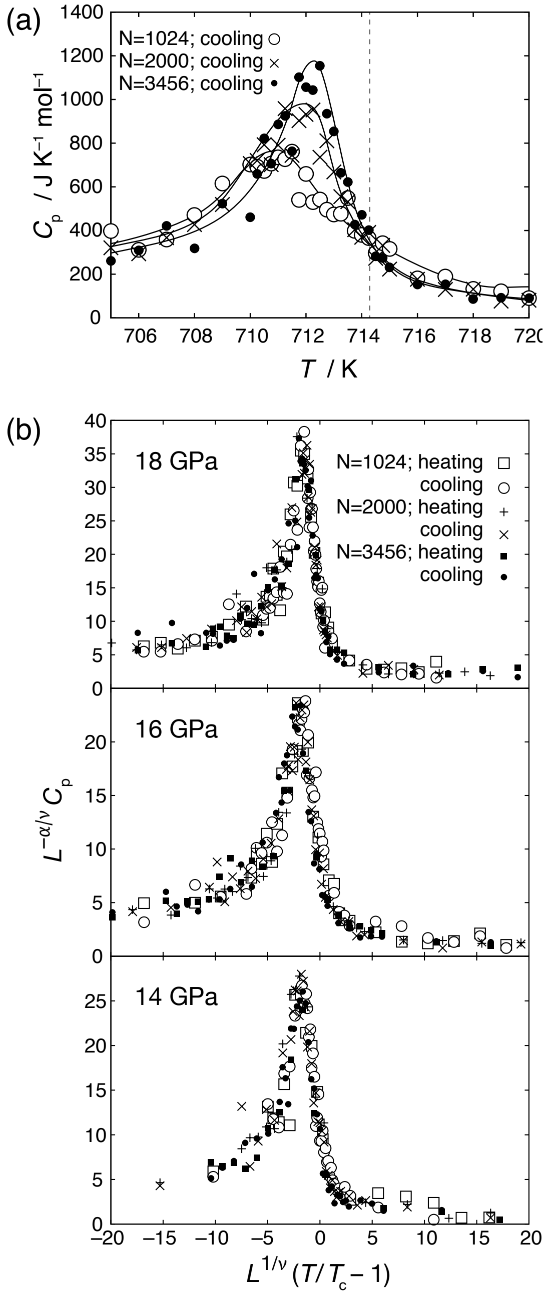

Figure 4.3 | Second-order phase transition

(a) The heat capacity at constant pressure (C_p) at the second-order phase transition. Pressure is 16 GPa. Open circles, crosses, and dots correspond to systems of size N=1024, 2000, and 3456, respectively. Dashed line indicate T_c($N = \infty$) estimated by finite size scaling technique. Solid curves are for eye guide.

(b) The scaled heat capacities at 14, 16, and 18 GPa against the scaled reduced temperature, which are based on the scaling hypothesis Eq. 4.3 in Methods section. Here, ν and α are the critical exponents for the correlation length and for C_p, respectively. We get ν by the finite-size scaling technique (see Methods section) and α by fitting $C_p(T)$ with the relation $C_p \sim | T/T_c - 1 |^{-\alpha}$ (written in the text in more detail; see Fig. 4.4(c)). Estimated values of T_c, ν, and α at each pressure are tabulated in Table 4.2.

The results mentioned so far make us find that the first-order phase transition line continuously gives way to the second-order one as the pressure increases. The Landau theory tells us the tricritical point should intervene between the two types of phase transition line. Pressure dependence of the spinodal lines in Fig. 4.1(b) suggests the singularity at around 13.3 GPa, nevertheless scaling behavior seems to persist even at subcritical pressures because of the finite system size.

In determining the critical point at each pressure, we first apply the finite size scaling technique to the Binder parameter to obtain the critical temperature at thermodynamic limit, $T_c(N = \infty)$, and the critical exponent ν for correlation length (see Methods section). The estimated critical line above the tricritical point at 13.3 GPa is also shown in Fig. 4.1. We then assess three other critical exponents α, β, and γ, for C_p, ϕ, and thermal fluctuation of ϕ (χ_ϕ), respectively, using the system of size N=3456. Their asymptotic behaviors, $C_\mathrm{p} \sim |\epsilon|^{-\alpha}$, $\phi \sim |\epsilon|^{\beta}$, and $\chi_\phi \sim |\epsilon|^{-\gamma}$, where $\epsilon \equiv T/T_\mathrm{c} - 1$ is the reduced temperature, allow us to estimate them by regression method. Divergent behaviors of these quantities and their linear approximations are shown in Fig. 4.4(a). Estimated critical temperatures and exponents are listed in Table 4.2 [63–66]. Critical exponents are found to be almost independent from pressure. These values are different from the critical exponents for 3-dimensional Ising model, and rather close to the numerically estimated tricritical exponents of Blume-Capel spin-1 Ising model and those determined experimentally for ammonium chloride crystal, which also exhibit the crossover from first- to second-order phase transitions. At 26 GPa, which is the highest pressure in the present work, the exponents slightly shift to those for 3D Ising critical point. Note that all the obtained exponents above 10 GPa roughly obey Rushbrooke's scaling law [67]: $\alpha + 2\beta + \gamma = 2$ (Fig. 4.4(b)).

Table 4.2 | Critical temperature and exponents

Pressure / GPa	$T_c(N=\infty)$ / K	α $T < T_c$	β $T < T_c$	γ $T < T_c$	ν	$\alpha+2\beta+\gamma$
26	855.0(2)	0.41(3)	0.179(1)	1.03(4)	0.55(4)	1.81(5)
18	746.5(2)	0.53(4)	0.172(1)	1.16(5)	0.58(4)	2.04(6)
16	714.3(2)	0.59(4)	0.165(1)	1.09(5)	0.55(4)	2.01(7)
14	679.5(2)	0.58(3)	0.157(2)	1.16(3)	0.55(5)	2.05(4)
13*	660.2(2)*	0.60(4)	0.152(1)	1.18(4)	0.55(7)	2.08(6)
12	640.3(2)	0.63(5)	0.139(1)	1.12(6)	0.55(7)	2.03(8)
11	619.8(1)	0.61(3)	0.132(1)	1.09(3)	0.55(6)	1.96(4)
10	597.1(3)	0.58(4)	0.123(1)	1.13(6)	0.55(11)	1.95(7)
Critical point by mean field approx.		0	1/2	1	1/2	2
Tricritical point by mean field approx.[a]		1/2	1/4	1	1/2	2
Tricritical point of Blume-Capel model[b]		0.6	0.26	1.12	0.505	2.24
Tricritical point of NH_4Cl by experiment		0.57[d]	0.16[c]			

a Ref. 28

b Ref. 29

c Ref. 30

d Ref. 31

* Closest data point to the estimated tricritical point (13.3 GPa, 665 K).

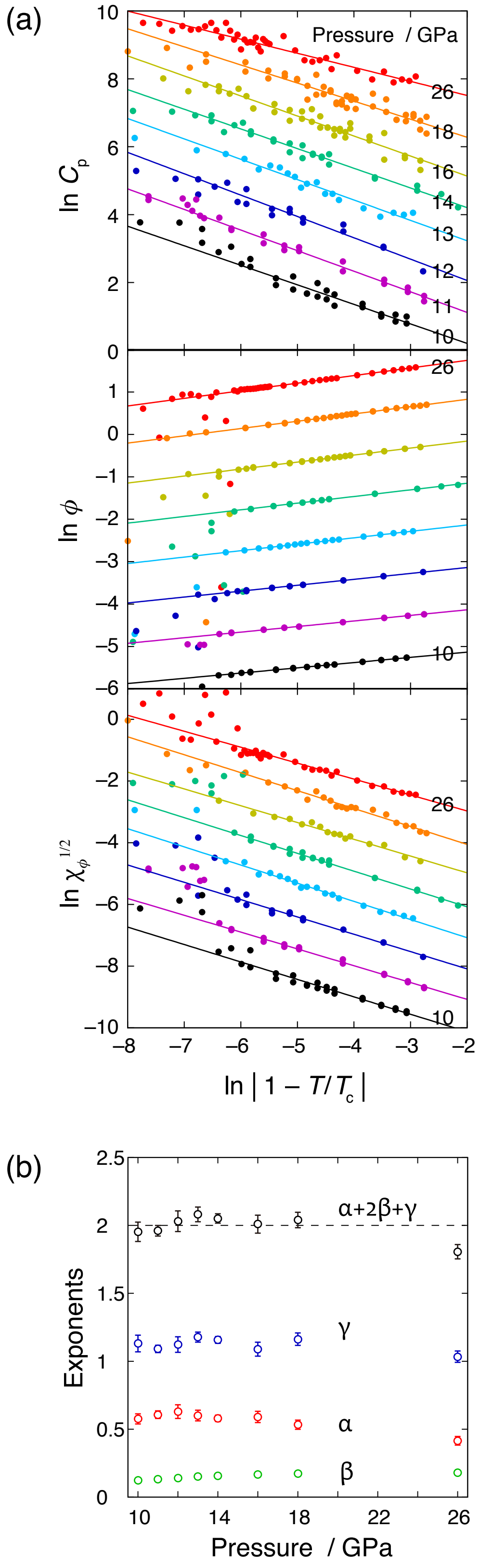

Figure 5.4 | Asymptotic behavior of physical properties in the vicinity of the critical point

(a) Heat capacity at constant pressure (C_p), order parameter of the system (ϕ), and fluctuation of ϕ (χ_ϕ) are plotted against the reduced temperature $T/T_c(N) - 1$ below the temperature of the maximum C_p in finite size system, $T_c(N)$, in log-log plot. The system size is $N = 3456$. The fitting lines embody the critical exponents.

(b) Plots of estimated critical exponents α, β, γ, and their sum, $\alpha + 2\beta + \gamma$, against temperature. Dashed line indicates Rushbrooke's scaling law: $\alpha + 2\beta + \gamma = 2$.

Extrapolation of spinodal lines suggests that the tricritical point for TIP5P-E water model resides at around (T, p) = (665 K, 13.3 GPa). However, we should be careful enough to tell where the actual tricritical point is, since even the phase transition between ice VII and plastic ice has not been observed experimentally, and also the water model is not designed so as to reproduce the properties of water at such high pressures and temperatures precisely. We just anticipate that the critical fluctuations may give us clue for determining the phase boundary between them by experiments. (Comparison with the precedent researches is made in Appendix for Chapter 4. See Fig. A4.2.) Theoretical studies also predict the plastic ice polymorphs of close-packed structure at the present thermodynamic conditions [16]. However, structural phase transition from ice VII has not been identified experimentally. More careful surveys are awaited both experimentally and theoretically.

Note that similar phase behavior was also observed in the case of order-disorder phase transition in NH_4Cl crystal [68]. The phase transition between a disordered phase II and an ordered phase IV of NH_4Cl is first-order below the tricritical point at 1.5 GPa and second-order above it. In the phase transition from II to IV, NH_4Cl crystal acquires tetrahedral symmetry by fixing the orientation of NH_4^+ ion, similarly to the case of plastic to VII phase transition where orientations of water molecules are fixed and the crystal acquires tetrahedral symmetry. It is therefore worthwhile to address a similarity and a difference between ice VII and ammonium halide. The structures of both crystals have tetrahedral arrangement doubly degenerated in the spatial orientation of protons. It is this degeneracy that gives rise to the sixth-order polynomial of an appropriately chosen order parameter in the Landau free energy, which is, in turn, an origin of the tricritical point and the phase boundary of second-order transition. The disordered phase of ammonium halide is still crystalline but the corresponding phase in ice VII is plastic where the reorientational motion is much faster than that in the crystalline form. This difference seems to be elucidated in the following way. The cohesion energy to form the crystal in ammonium halide is mainly due to the Coulombic interaction between two sorts of ions and the orientational order is governed by a different interaction from the cohesive energy. On the other hand, both cohesion energy and orientational ordering are dominated by hydrogen bonds in ice VII. The orientational disordering in ice VII necessarily accompanies breaking of a fairly large number of hydrogen bonds while keeping the basic lattice structure intact because of high pressure. (This situation should be distinguished from occasional breakdown and recovery of local hydrogen bond network involving only several molecules, which may take place even at a low temperature.) Such a disordering in ammonium halide is caused by a rather small amount of energy compared with the ionic interaction and therefore the transition is observed at low temperatures. This difference could be a main source of appearance of the plastic phase in ice VII. The role of hydrogen bonds becomes less significant with increasing the pressure (density) and this leads to vanishing the first-order transition under high pressure. That is, compression undermines the tetrahedral coordination of hydrogen bonds and the packing effect gradually prevails so that the second-order transition takes over the first-order one.

We should also mention that we limit our calculation up to 26 GPa because of the reliability of rigid TIP5P-E water model. Experimentally, ice VII changes to ice X at 62 GPa and ambient temperature, in which the OH bond is symmetrized [69]. The energy barrier for proton hopping in ice VII will become lower from much lower pressure than the VII-X phase boundary, but rigid water models cannot deal with the migration of hydrogen atoms. It is of interest how the critical line approaches and connects to the phase boundary with ice X, and how the critical behavior changes accordingly. The phase behaviors of ice VII and plastic ice at higher pressure should be investigated by more realistic method, such as the *ab initio* MD technique.

We want to stress the importance of analyzing the critical phenomena of molecular system. Several decades' researches on critical phenomena by computer simulations have been devoted mainly on spin models. However, phase diagram of the real material is more complicated than that of spin models, and the critical point is usually not isolated on the phase diagram. Critical fluctuation may affect the adjacent phase transition. Even the metastable critical point might play very important roles in phase behavior, as we learnt from the studies on second critical point of water [70]. Water has many polymorphs and many other order-disorder phase transitions according to the proton disorder. There might be another criticality yet to be discovered.

Appendix for Chapter 4

Estimation of spinodal and coexistence temperatures via polynomial fitting of Landau free energy functional.

Here we describe the method to estimate the spinodal and coexistence temperatures at a given pressure by fitting the Landau free energy functional with a 6th-order even polynomial, which is defined as a functional of the order parameter ϕ as follows:

$$\begin{aligned} g(\phi) &= r'\phi^2 + u_4'\phi^4 + u_6\phi^6 \\ &= u_6\left(\frac{r'}{u_6}\phi^2 + \frac{u_4'}{u_6}\phi^4 + \phi^6\right) \\ &= u_6(r\phi^2 + u_4\phi^4 + \phi^6), \end{aligned} \tag{A4.2}$$

where we redefine the coefficients as $r = r'/u^6$ and $u_4 = u_4{}'/u^6$. We assume u_6 is always positive by stability condition. When $u_4 < 0$, this polynomial has three minima at $\phi \leq 0$ and at two non-zero ϕ values with different sign. Differentiation of this polynomial readily tells us that the coexistence of the three states, i.e., the condition where the values at three minima are the same, occurs when $r = u_4/4$, and the spinodal points correspond to the condition where the number of minima changes, which occurs when $r = 0$ or $r = u_4^2/3$.

Therefore, when the values $r - u_4/4$, r, and $r - u_4/3$ are plotted against temperature, their intersection points with the *x* axis (temperature axis) correspond to the unbiased estimates of the coexistence and two spinodal temperatures, respectively. With the real data obtain by the simulation, the se values change almost linearly against temperature in the vicinity of the phase boundary and therefore we can estimate the intersection points fairly precisely. Fig.A4.1 illustrates the actual process of estimating these temperatures.

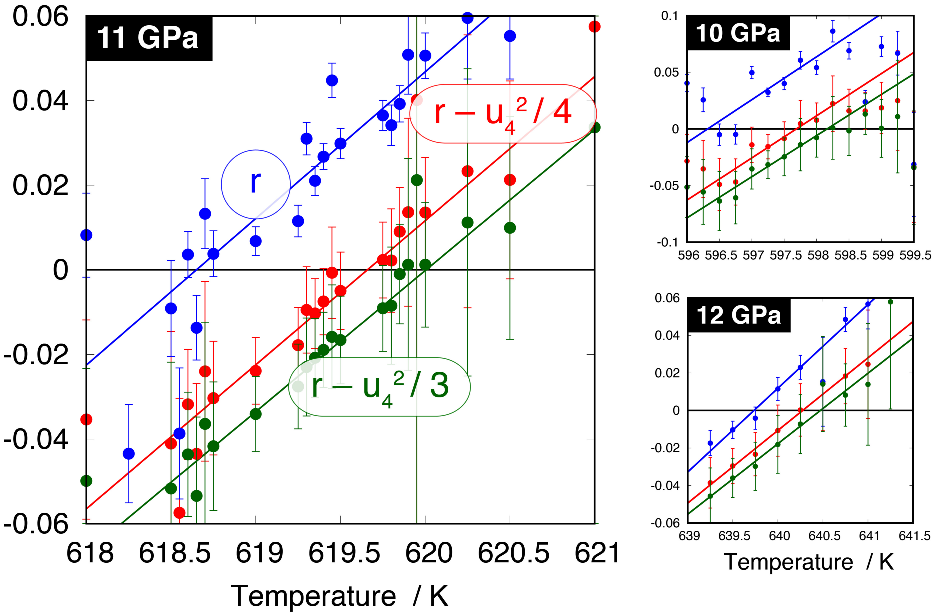

Figure A5.1

Blue, red, and green points are values r, $r-u_4/4$, and $r-u_4/3$ obtained by fitting the Landau free energy functional with 6th-order even polynomial (Eq. A4.1), respectively. Intersection points of the linear fitting lines of them with the abscissa axis give the unbiased estimates of spinodal and coexistence temperatures. Pressures are 10, 11, and 12 GPa.

When r changes linearly and u_4 is constant against temperature, we obtain a simple relation between coexistence temperature T_c and lower and higher spinodal temperatures T_0 and T_1, that is

$$T_\mathrm{c} - T_0 = 3(T_1 - T_\mathrm{c}). \tag{A4.2}$$

Actually, one can see this relation approximately holds at the pressures between 10 and 12 GPa in Fig. 4.1(b). We therefore also make use of this relation to estimate the coexistence temperature from two spinodal temperatures below 10 GPa where determination of coexistence temperature by direct molecular dynamics simulation is difficult.

Comparison with experimental data.

Shown in Fig. A4.2 are the phase boundaries between ice VII and supercritical fluid water determined by experiments [3–10] and by computer simulations [13,16]. Note that the phase boundaries obtained by Takii et al. [13] and by Aragones et al. [16] by computer simulations have two branches corresponding to fluid-plastic and plastic-VII transitions.

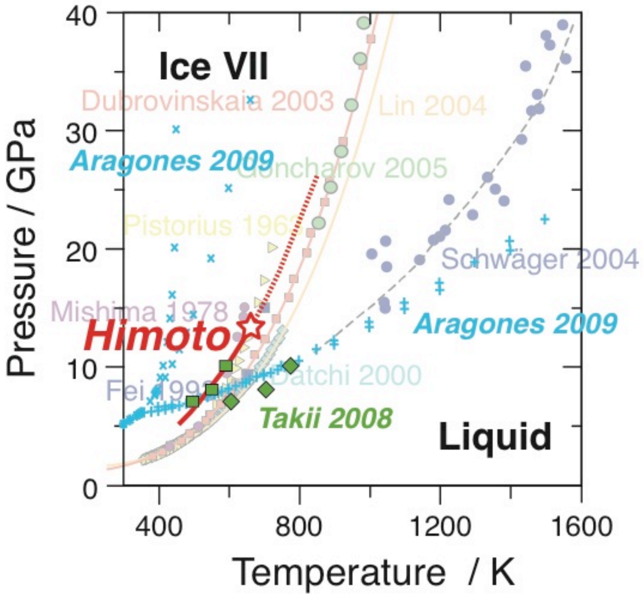

Figure A5.2 | Phase boundaries between ice VII and the supercritical fluid water

Takii (the water's potential model is TIP5P) [13], Aragones (TIP4P/2005) [16], and Himoto's data (the present work; TIP5P-E model) are obtained by computer simulations; other data are by experiments [3–10]. Takii and Aragones' data include the melting points of plastic ice to the fluid water. The red star in Himoto's series indicates the pressure and temperature of the tricritical point discovered in the present work.

References

[1] C. G. Salzmann, P. G. Radaelli, B. Slater, and J. L. Finney, Phys. Chem. Chem. Phys. **13**, 18468 (2011).

[2] C. Salzmann, P. Radaelli, E. Mayer, and J. Finney, Phys. Rev. Lett. **103**, 105701 (2009).

[3] F. Datchi, P. Loubeyre, and R. LeToullec, Phys. Rev. B **61**, 6535 (2000).

[4] N. Dubrovinskaia and L. Dubrovinsky, High Press. Res. **23**, 307 (2003).

[5] Y. Fei, H. Mao, and R. J. Hemley, J. Chem. Phys. **99**, 5369 (1993).

[6] A. Goncharov, N. Goldman, L. Fried, J. Crowhurst, I.-F. Kuo, C. Mundy, and J. Zaug, Phys. Rev. Lett. **94**, 125508 (2005).

[7] J.-F. Lin, B. Militzer, V. V Struzhkin, E. Gregoryanz, R. J. Hemley, and H. Mao, J. Chem. Phys. **121**, 8423 (2004).

[8] O. Mishima and S. Endo, J. Chem. Phys. **68**, 4417 (1978).

[9] C. W. F. T. Pistorius, M. C. Pistorius, J. P. Blakey, and L. J. Admiraal, J. Chem. Phys. **38**, 600 (1963).

[10] B. Schwager, L. Chudinovskikh, A. Gavriliuk, and R. Boehler, J. Phys. Condens. Matter **16**, S1177 (2004).

[11] P. W. Bridgman, J. Chem. Phys. **5**, 964 (1937).

[12] M. R. Frank, Y. Fei, and J. Hu, Geochim. Cosmochim. Acta **68**, 2781 (2004).

[13] Y. Takii, K. Koga, and H. Tanaka, J. Chem. Phys. **128**, 204501 (2008).

[14] R. Brand, P. Lunkenheimer, and a. Loidl, J. Chem. Phys. **116**, 10386 (2002).

[15] J. L. Aragones, M. M. Conde, E. G. Noya, and C. Vega, Phys. Chem. Chem. Phys. **11**, 543 (2009).

[16] J. L. Aragones and C. Vega, J. Chem. Phys. **130**, 244504 (2009).

[17] F. Stillinger and T. Weber, **87**, 2833 (1983).

[18] I. Ohmine and H. Tanaka, Chem. Rev. **93**, 2545 (1993).

[19] M. Matsumoto, J. Chem. Phys. **126**, 054503 (2007).

[20] W. L. Jorgensen, J. Chandrasekhar, J. D. Madura, R. W. Impey, and M. L. Klein, J. Chem. Phys. **79**, 926 (1983).

[21] J. L. F. Abascal and C. Vega, J. Chem. Phys. **123**, 234505 (2005).

[22] M. W. Mahoney and W. L. Jorgensen, J. Chem. Phys. **112**, 8910 (2000).

[23] S. W. Rick, J. Chem. Phys. **120**, 6085 (2004).

[24] C. G. Salzmann, P. G. Radaelli, A. Hallbrucker, E. Mayer, and J. L. Finney, Science **311**, 1758 (2006).

[25] C. G. Salzmann, A. Hallbrucker, J. L. Finney, and E. Mayer, Phys. Chem. Chem. Phys. **8**, 3088 (2006).

[26] V. F. Petrenco and R. W. Whitworth, *Physics of Ice* (Oxford University Press, 1999).

[27] J. Besson, P. Pruzan, S. Klotz, and G. Hamel, Phys. Rev. B **49**, 540 (1994).

[28] M. Song, H. Yamawaki, H. Fujihisa, M. Sakashita, and K. Aoki, Phys. Rev. B **68**, 024108 (2003).

[29] K. Umemoto, R. M. Wentzcovitch, S. de Gironcoli, and S. Baroni, Chem. Phys. Lett. **499**, 236 (2010).

[30] L. Liu, Earth Planet. Sci. Lett. **61**, 359 (1982).

[31] Y. Asahara, K. Hirose, Y. Ohishi, N. Hirao, and M. Murakami, Earth Planet. Sci. Lett. **299**, 474 (2010).

[32] H. Tanaka, J. Mol. Struct. THEOCHEM 561 (1999).

[33] N. G. Parsonage and L. A. K. Sataveley, *Disorder in Crystals* (Clarendon Press, Oxford, 1978).

[34] H. Berendsen, J. Phys. Chem. **91**, 6269 (1987).

[35] L. X. Dang, J. Chem. Phys. **97**, 2659 (1992).

[36] I. Ohmine, H. Tanaka, and P. G. Wolynes, J. Chem. Phys. **89**, 5852 (1988).

[37] M. P. Allen and D. J. Tildesley, *Computer Simulation of Liquids* (Oxford University Press, 1987).

[38] H. Tanaka, Phys. Rev. Lett. **80**, 113 (1998).

[39] D. Stauffer, *Introduction to Percolation Theory* (Tailor and Francis, London and Philadelphia, 1985).

[40] O. Mishima, J. Chem. Phys. **100**, 5910 (1994).

[41] K. Himoto, M. Matsumoto, and H. Tanaka, Phys. Chem. Chem. Phys. **13**, 19876 (2011).

[42] S. Nosé, J. Chem. Phys. **81**, 511 (1984).

[43] W. G. Hoover, Phys. Rev. A **31**, 1695 (1985).

[44] H. C. Andersen, J. Chem. Phys. **72**, 2384 (1980).

[45] F. Starr, J. Nielsen, and H. Stanley, Phys. Rev. E. Stat. Phys. Plasmas. Fluids. Relat. Interdiscip. Topics **62**, 579 (2000).

[46] Y. L. a. Rezus and H. J. Bakker, J. Chem. Phys. **123**, 114502 (2005).

[47] A. Einstein, Ann. Phys. **2**, 237 (1905).

[48] C. J. Fecko, J. J. Loparo, S. T. Roberts, and A. Tokmakoff, J. Chem. Phys. **122**, 54506 (2005).

[49] E. Abramson, Phys. Rev. E **76**, 051203 (2007).

[50] V. E. Petrenko and M. L. Antipova, Struct. Chem. **22**, 471 (2011).

[51] D. van der Spoel, P. J. van Maaren, and H. J. C. Berendsen, J. Chem. Phys. **108**, 10220 (1998).

[52] L. M. Prockter, Johns Hopkins APL Tech. Dig. **26**, 175 (2005).

[53] L. Landau, Zh. Eksp. Teor. Fiz. **7**, 19 (1937).

[54] O. Mishima and H. E. Stanley, Nature **396**, 329 (1998).

[55] P. H. Poole, F. Sciortino, U. Essmann, and H. E. Stanley, Nature **360**, 324 (1992).

[56] K. Stokely, M. G. Mazza, H. E. Stanley, and G. Franzese, Proc. Natl. Acad. Sci. U. S. A. **107**, 1301 (2010).

[57] Y. Liu, A. Z. Panagiotopoulos, and P. G. Debenedetti, J. Chem. Phys. **131**, 104508 (2009).

[58] D. van der Spoel, E. Lindahl, B. Hess, and The GROMACS development team, (n.d.).

[59] D. van der Spoel, E. Lindahl, B. Hess, and T. G. development Team, *GROMACS User Manual Version 4.6.1* (2013), pp. 67–73.

[60] J. M. Thijssen, *Computational Physics* (Cambridge University Press, Cambridge, 2007), p. 191.

[61] K. Binder, I. Festkrperforschung, and K. Jiilich, Z. Phys. B **140**, 119 (1981).

[62] P. M. Chaikin and T. C. Lubensky, *Principles of Condenced Matter Physics* (Cambridge University Press, Cambridge, 1995), pp. 172–174.

[63] F. J. W. Eberhard K. Riedel, Phys. Rev. B **9**, 294 (1974).

[64] D. M. Saul, M. Wortis, and D. Stauffer, Phys. Rev. B **9**, 4964 (1974).

[65] O. H. Seeck, D. Hupfeld, H. Krull, M. Tolan, and W. Press, **58**, 623 (1998).

[66] C. Garland and J. Baloga, Phys. Rev. B **16**, 331 (1977).

[67] G. S. Rushbrooke, J. Chem. Phys. **39**, 842 (1963).

[68] W. Yelon, D. Cox, P. Kortman, and W. Daniels, Phys. Rev. B **9**, 4843 (1974).

[69] K. Aoki, H. Yamawaki, M. Sakashita, and H. Fujihisa, Phys. Rev. B **54**, 673 (1996).

[70] L. Xu, I. Ehrenberg, S. V Buldyrev, and H. E. Stanley, J. Phys. Condens. Matter **18**, S2239 (2006).